New Zealand Journal of Geology and Geophysics

ISSN: (Print) (Online) Journal homepage: www.tandfonline.com/journals/tnzg20

Stratigraphy and lithosedimentological properties of subplinian eruptions from Mt. Taranaki, New Zealand, encompassed by the Ngaere and Pungarehu edifice collapses

Shannen Mills, Jonathan Procter, Anke Zernack & Stuart Mead

To cite this article: Shannen Mills, Jonathan Procter, Anke Zernack & Stuart Mead (29 Jan 2025): Stratigraphy and lithosedimentological properties of subplinian eruptions from Mt. Taranaki, New Zealand, encompassed by the Ngaere and Pungarehu edifice collapses, New Zealand Journal of Geology and Geophysics, DOI: 10.1080/00288306.2025.2454554

To link to this article: https://doi.org/10.1080/00288306.2025.2454554

NEW ZEALAND JOURNAL OF GEOLOGY AND GEOPHYSICS
https://doi.org/10.1080/00288306.2025.2454554

Taylor & Francis
Taylor & Francis Group

RESEARCH ARTICLE

OPEN ACCESS Check for updates

Stratigraphy and lithosedimentological properties of subplinian eruptions from Mt. Taranaki, New Zealand, encompassed by the Ngaere and Pungarehu edifice collapses

Shannen Mills, Jonathan Procter, Anke Zernack and Stuart Mead

Volcanic Risk Solutions, School of Agriculture and Environment, Massey University, Palmerston North, New Zealand

ABSTRACT

The sudden removal of large portions of a volcanic edifice through collapse can cause depressurisation in the subvolcanic magmatic system, influencing the nature of subsequent eruptions. At Mt. Taranaki, edifice failure has occurred frequently and at different timescales throughout the volcanic history, forming a broad pattern of cyclic collapse and regrowth. About 20–30,000 years ago, Mt. Taranaki experienced two such cycles in short succession, emplacing the 27.3 ka Ngaere and the 24.8 ka Pungarehu debris-avalanche deposits, which were preceded and followed by a sequence of twenty-eight closely spaced tephra deposits known as the Poto and Paetahi Formations. Here, we reconstruct the tephrastratigraphic framework of the Poto and Paetahi Formations, revealing a minimum total eruptive volume of 3 km^3. While eruptions directly following edifice failure were larger compared to those prior to collapse, this 4,000-year long eruptive period was characterised by consistently large subplinian eruptions. In contrast, large explosive events within the Holocene sequence are less frequent, with more multi-phase periods of effusive and explosive activity recorded. Our new data highlights the need to include longer-term eruptive records in volcanic hazard modelling since the most recent volcanic history might not cover the full nature of volcanic processes occurring at long-lived stratovolcanoes.

ARTICLE HISTORY
Received 8 May 2024
Accepted 7 January 2025

HANDLING EDITOR
Indranova Suhendro

KEYWORDS
Mt. Taranaki; andesite stratovolcano; subplinian eruption; tephra fall; edifice collapse

Introduction

The majority of stratovolcanoes around the world experience edifice or flank collapse events at least once during their lifetimes generating volcanic debris avalanches and in some cases tsunamis, which pose a major hazard to the surrounding areas (McGuire 1996; Siebert 1996; Voight and Elsworth 1997; Voight 2000; Girina 2013; Roverato and Dufresne 2021). Major edifice failures dramatically modify the morphology of the edifice; this can impact the eruption rate (frequency and/or magnitude), magmatic composition (e.g. Mt Pelée, Martinique (Germa et al. 2011; Boudon et al. 2013); Stromboli, Italy (Hornig-Kjarsgaard 1993; Petrone et al. 2009; Vezzoli et al. 2014)), or eruptive style as observed at some volcanoes globally (Siebert et al. 2004; Tibaldi 2004; Hora et al. 2009; Manconi et al. 2009; Zernack and Procter 2021), while other volcanoes experience no change in eruptive behaviour following collapse (e.g. Ponomareva et al. 2006; Zernack et al. 2012; Zernack and Procter 2021). The proximity of the failure to the source of magma can influence the response of the magmatic system influencing the eruption style, volcanoes can experience explosive activity (i.e. tephra fall, pyroclastic density currents and lateral blasts), through to effusive activity (i.e. lava flows and lava domes) (i.e. Fuego de Colima, Mexico, changing from effusive lava flows prior to collapse to explosive andesitic eruptions after collapse) (O'Callaghan and Francis 1986; Luhr and Prestegaard 1988; Robin et al. 1990; Stoopes and Sheridan 1992; Vallance et al. 1995; Siebert 1996; Vallance et al. 2001; Capra and Macías 2002; Pallister et al. 2017; Watt 2019). Generating accurate eruption scenarios for hazard mitigation from potential future eruptions requires an extensive understanding of the eruptive history of a volcano. However, due to better access and preservation of the younger records, most eruption histories for volcanoes worldwide are limited to the Holocene period. As a result, the effects of large (prehistoric) edifice collapse events on subsequent eruptive activity are still poorly understood (Watt 2019).

Over the last ~300 years, globally, five collapse events >1 km^3 have been observed, including Oshima-Oshima, Japan in1741 CE (Katsui and Yamamoto 1981; Satake and Kato 2001; Satake 2007); Ritter Island, Papa New Guinea in 1888 CE (Johnson 1987; Day et al. 2015; Karstens et al. 2019); Bandai, Japan

CONTACT Shannen Mills s.mills@massey.ac.nz

in 1888 CE (Yamamoto et al. 1999; Yoshida 2013); Shiveluch, Kamchatka in 1964 CE (Belousov 1995; Ponomareva et al. 2006) and Mount St. Helens, U.S.A in 1980 CE (Voight et al. 1983; Glicken 1996). Within the geological record over 300 collapse events have been identified in depositional sequences at over 200 volcanoes (Watt 2019). Changes in eruptive behaviour or magmatic composition following edifice collapse events have been observed for nine pre-Holocene collapse events, i.e. 16–10 ka Shiveluch, Kamchatka, 126 ka Coni/Pelée, Martinique, 14 ka Stromboli, Italy, 65–60 ka Chimborazo, Ecuador, and 35–60 ka Mt. Taranaki, New Zealand (Watt 2019; Zemeny et al. 2023). Complementary to this, eight collapse events have recorded a change in eruptive behaviour or magmatic composition within the Holocene, i.e. 3 ka Tungurahua, Ecuador (Hall et al. 1999), ~6 ka Tata Sabaya, Bolivia (de Silva et al. 1993), and 1888 CE Ritter Island, Papa New Guinea (Johnson 1987; Day et al. 2015; Karstens et al. 2019). Understanding the influence collapse has on volcanological processes requires detailed tephrochronological analysis, which typically focus on better preserved Holocene records with limited studies existing on pre-Holocene events.

At Mt. Taranaki, the long-term (200 kyr) volcanic history and predominant landscape-forming processes have been reconstructed based on volcaniclastic records preserved in the surrounding ring plain (Neall 1979; Alloway et al. 1995; Procter et al. 2009; Zernack et al. 2009, 2011; Zemeny et al., 2021; Zernack, 2021). These studies have shown that one of the major hazards at Mt. Taranaki is edifice failure with fourteen major collapses recognised in its eruptive history (Zernack et al. 2011; Zernack et al. 2012). Yet only data on eruptive behaviour and changes in the patterns of eruptive styles of the last 5,000 years (Platz et al. 2007; Turner et al. 2008; Torres-Orozco et al. 2018; Lerner et al. 2019c) were used to generate future hazard scenarios from the volcano (Weir et al. 2022). This period is too short to encompass the much longer timeframes of Mt. Taranaki's cyclic growth and collapse behaviour. It also ignores the volcano's history of frequent edifice failure and the impacts such large-scale events have on the subvolcanic plumbing system and eruptive behaviour, with the last event, the 7.5 ka Opua collapse, pre-dating this framework by more than 2,000 years.

In this study, we focused on the 23.1–27.3 ka ringplain succession to extend our understanding of Mt. Taranaki's cyclic volcanic history past the well-studied Holocene record (<12 ka). The studied interval is characterised by two temporally proximal large edifice collapse events that emplaced the 27.3 ka (5.85 km^3) Ngaere and 24.8 ka (>7.5 km^3) Pungarehu debris-avalanche deposits (DADs). Eruptive activity preceding and following these collapse events produced a series of tephra deposits, the Poto and Paetahi Formations. In contrast to many volcanoes worldwide, where eruptive sequences around DADs are poorly preserved or inaccessible, Mt. Taranaki thus provides a unique opportunity to investigate the response of a long-lived stratovolcano to repeated large edifice collapse.

Methodology

The Poto and Paetahi tephra beds were initially identified on the southeastern ring plain interbedded with andic paleosols (Alloway et al. 1995), with this study adding further localities across a wide east to southeastern arc between 11 and 45 km from the present-day summit vent (Figure 1). Deposits across the northeastern sector of the ring plain have been buried underneath younger deposits and removed or buried by industrialisation limiting their preservation. Previously identified deposits in the northeast by Alloway et al. (1995) were no longer exposed or accessible in the field. Because of this, these deposits have not been used in volume calculations or isopach maps in this study. For this study, extended locations were used to correlate individual depositional layers across the Taranaki region. These were identified through differences in lithosedimentological characteristics that distinguished them from the surrounding layers (Ingram 1954; Fisher and Schmincke 1984; Cas and Wright 1987) with boundaries being marked by either a sharp or blurred contact. Lithosedimentological characteristics include juvenile and lithic clasts proportions, grain size, sorting, bedding, deposit geometry, and presence and nature of enclosing paleosols.

Eruptive events were divided into single-phase (individual events) or multi-phase (multiple events) based on their depositional characteristics (e.g. Voloschina et al. 2020), which were classified as below.

- Single-phase (SB) layers appear in pockets within the stratigraphy creating a wavy appearance with boundaries characterised by paleosols or distinct/blurred contacts between depositional units. Internal variations are not quantifiable within the individual layers. Some layers have distinguishable features in relation to others, which assist with correlations of single-phase events between locations.
- Multi-phase (MB) layers were originally recognised as single bed layers with internal stratification (e.g. Paetahi.a was referred to as having shower bedding by Alloway et al. 1995). These units have been reclassified as multi-phase layers within this study as they showed internal depositional variations in lithology, grain size, deposit texture, or colour (e.g. Voloschina et al. 2020). These deposits are

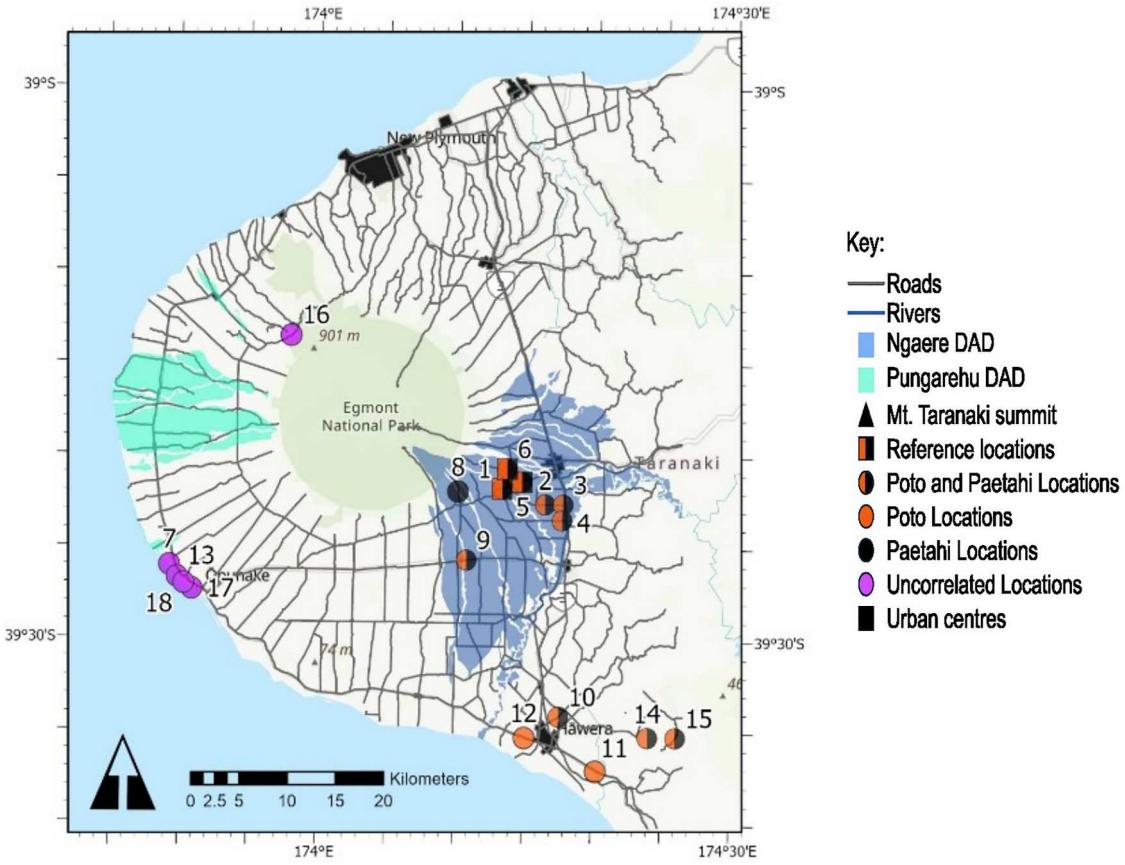

Figure 1. Field location map of the Poto and Paetahi Formations across the Taranaki ring plain. Road and Topographic data sourced from the Land Information New Zealand (LINZ) Data Service licensed for reuse under CC by 4.0.

recognisable in the same stratigraphic sequence with no shifting in stratigraphic position of the layers across the ring plain compared with shower bedding, where interlinking of the layers between locations is expected. These multi-phase layers are found across the eastern and southeastern sectors of the Taranaki ring plain either as complete stratigraphic set (lower to upper units) or as individual subunits.

Depositional characteristics of each layer were recorded, including consolidation, grain size characteristics (Wentworth 1922; Fisher and Schmincke 1984; Cas and Wright 1987; White and Houghton 2006), grading, sorting, componentry, thickness, and upper and lower contacts (Fisher and Schmincke 1984; Cas and Wright 1987; Torres-Orozco et al. 2017a). Further grain-size analysis and point counts were performed on depositional units from the Poto and Paetahi reference locations (Figure 1; location 1 Ronald Road 39°21′41.64″S; 174°13′20.02″E; location 5 Opunake Road 39° 21′21.45″S; 174°14′38.09″E; location 6 Paetahi Stream 39°20′34.71″S; 174°13′41.90″E). Manual dry sieving at 0.5 ϕ intervals between −4 and 4 ϕ was conducted, and individual grain sizes were weighed and normalised to 100. Statistical parameters (Folk and Ward 1957) for grain size were obtained through GradiSTAT (Blott and Pye 2001) using a size scale modified after Udden (1914) and Wentworth (1922).

The −1.5 and 0.5ϕ size fractions were chosen for componentry analysis, allowing comparison between dominant lapilli-bearing deposits and finer-grained ash beds. On average, at least 300–500 grains were used for point count analyses, although for some layers it was less for the −1.5 ϕ class size due to a lack of coarser particles. The percentages of individual componentry classes were calculated relative to the total number of grains counted, distinguishing between juveniles (primary erupted material), lithics (secondary material brought up during the eruptions, including older eruptive products and other lithologies that make up the conduit and subvolcanic basement (Sparks 1976; Fisher and Schmincke 1984; Carey and Houghton 2010; Campbell et al. 2013; Paredes-Mariño et al. 2019)), and free crystal components, (i.e. matrix-free crystals generated through the fragmentation of crystal-rich pumices during the eruptive phase (Sparks 1976; White and Houghton 2006; Paredes-Mariño et al. 2019)). Clast classes were further divided into subgroups: two juvenile classes (1. Grey pumice, 2. Brown pumice), four lithic classes (3. Altered pumice, 4. Grey lithics, 5. Altered lithics, 6. White claystone), and four free crystal classes (7.

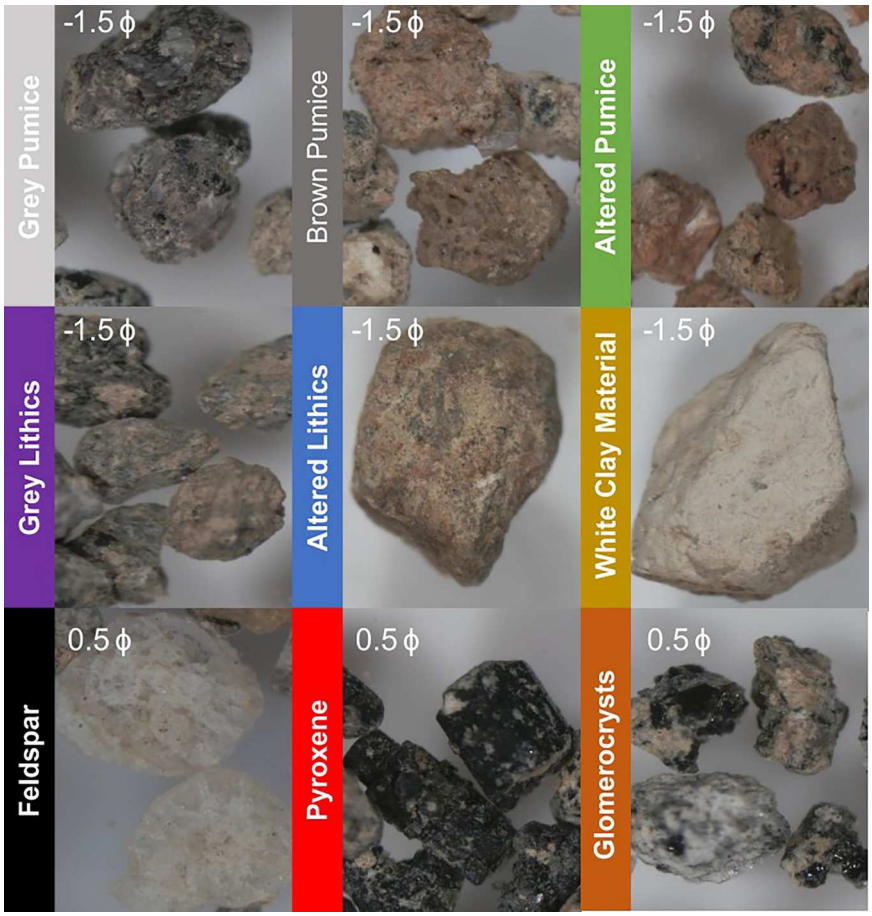

Figure 2. Images of the different components present within the Poto and Paetahi tephras. Grains are from the−1.5θ and 0.5θ size fraction.

Feldspars, 8. Pyroxenes, 9. Amphiboles and 10. Glomerocrysts) (Figure 2).

Volume estimates for individual layers were calculated using the Weibull model (Bonadonna and Costa 2012; Bonadonna and Costa 2013) produced in AshCalc (Daggitt et al. 2014) using the equation ($T\,x = \theta\left(\frac{x}{\lambda}\right)^{k-2} e\left(\frac{x}{\lambda}\right)^{k}$) where the thickness ($T$) is related to the square root of the isopach area (x). Input parameters for the model are isopach thickness (m) and $\sqrt{}$Area (km) ($A^{1/2}$). This model has incorporated λ as a parameter to allow for the variation in thinning rate that is seen in tephra deposits with multiple segments (Daggitt et al. 2014), which works well with the more medial and distal deposits due to a decrease in thickness with distance from the source (Bonadonna and Costa 2012; Bonadonna and Costa 2013). Eruption column heights (Ht) were calculated using the Mastin et al. (2009) equation ($H = 25.9 + 6.64\log_{10}(V)$). The total erupted mass (mT) was calculated after the equation (volume * 1000 kg/m^3) from Wilson (1976). Mass eruption and discharge rates (MER and Q) were calculated using methods from Sparks (1976) and Mastin et al. (2009). Eruptive magnitudes were calculated using equations (mass/ (rock density) $*1^{-9}$) and log10 ($\log^{10}(\text{DRE[kg]})^{-7}$) from Pyle (2000). To estimate the minimum duration (hours) of the eruption, the equation ((mT/MER) *3600) from Wilson (1976) was used.

Multiple models are used for calculating the volume of ash produced during an eruptive event, e.g. Exponential (Pyle 1989), Power law (Bonadonna et al. 1998; Bonadonna and Houghton 2005), and Weibull (Bonadonna and Costa 2012). The volume of a deposit can be significantly underestimated when either proximal, medial, or distal regions are missing (Pyle 1989; Fierstein and Nathenson 1992; Rose 1993; Pyle 1995; Bonadonna and Costa 2012). For datasets where large sections of the deposit are missing, the Weibull model provides the smallest uncertainties compared to other models, which extrapolate areas of missing data (Bonadonna and Costa 2012; Bonadonna and Costa 2013). Reducing uncertainties at this step is important to decrease the amount of uncertainty for other eruptive parameters, which are all calculated using eruptive volumes. Although our proximal data is missing, the medial and distal data was robust enough to apply the Weibull model through AshCalc (Bonadonna and Costa 2012; Daggitt et al. 2014).

Column height calculations using the methods of Mastin et al. (2009) and the Carey and Sparks (1986) model for the same isopach data produced

considerable differences in column heights (e.g. 18.67 vs. 30.1 km, respectively). These discrepancies indicate the levels of uncertainty associated with studying prehistoric eruptive events. This study determined that the values generated using Mastin et al. (2009) provided more reliable heights for the Poto and Paetahi eruptive events in the context of global examples (Thorarinsson and Sigvaldason 1972; Sarna-Wojcicki 1981; Carey and Sigurdsson 1985; Fierstein and Nathenson 1992; Gudmundsson et al. 1992; Rosi et al. 1993; Cole et al. 1995; Höskuldsson et al. 2007; Carey and Houghton 2010).

Results

Revised stratigraphy of the Poto and Paetahi Formations

The Poto Formation occurs across the eastern, southeastern, and southwestern ring plain (Figure 1; supplementary material Table 1) (Alloway et al. 1995), with nineteen depositional layers (Figure 3; Table 1) being preserved at the Poto reference section (Figure 1, location 1). At the base of the sequence, two layers of ash and lapilli fall (Poto.a and Poto.b) are found below the Ngaere DAD. Four layers of ash and lapilli (Poto-c. l to e) and one surge deposit (situated above Poto.e) occur above the Ngaere DAD and are overlain by the 25.4 ka rhyolitic Kawakawa-Oruanui tephra (Figure 3) (c.f., Vandergoes et al. 2013). Situated above the Kawakawa-Oruanui tephra are twelve ash and lapilli layers (Poto.f to o) (Figure 3).

The Paetahi Formation is separated from the Poto Formation below by a 6 cm thick well defined paleosol. The Paetahi Formation is found in southeast Taranaki (Alloway et al. 1995) and comprises ten ash and lapilli layers (Figure 4; Table 2). The reference section for the lower six (Paetahi.a l to d) layers is situated along Opunake Road west of Stratford and the reference section for the upper four layers (Paetahi.e l to f) is located along Cardiff Road on the southern side of Paetahi Stream (Figure 1, locations 5 and 6 respectively).

This study expanded the stratigraphy of the Poto and Paetahi Formations by identifying single-phase and multi-phase layers based on depositional characteristics. This has added three new subunits to the Poto Formation (Poto.c upper, k upper and l upper) and four to the Paetahi Formation (Paetahi. a middle, a upper, e middle and e upper) (Table 3). The units are layers of ash and lapilli fall with one surge deposit located directly above Poto.e at the reference section (Figure 3; Table 1). Poto.i was described as a thin surge bed based on sorting and the occurrence of cross laminations by Alloway et al. (1995). This study has reclassified Poto.i as a fall due to its appearance within pockets across the outcrop, absence of bedding features and moderate sorting, containing pumice and lithic clasts.

The Poto Formation is dominated (66%) by single-phase (SB) events compared to the Paetahi Formation where most (60%) are multi-phase eruptions (Figures 5 and 6).

The multiphase Paetahi Formations have similar depositional characteristics however, Paetahi.a middle contains more grey pumice while Paetahi.e middle contains more lithic clasts than the lower and upper units. The upper beds record a shift back to an orange pumice-dominated layer, with Paetahi.a upper being unconsolidated while Paetahi.e upper is strongly consolidated. Paetahi.e middle is the most widely distributed layer of the Paetahi.e multi-phase event.

Most Poto layers are contained within a yellow-brown consolidated clay-rich paleosol. The single-phase Paetahi layers are found within a consolidated clay-rich material containing a larger number of soft pumices than the multi-phase Paetahi layers.

The two multi-phase events of the Paetahi Formation protrude out of the outcrop and appear to weather less easily compared to the surrounding layers, which results in being more easily recognised and correlated across the ring plain (Fence diagram in supplementary material Figures 1 and 2). The upper boundary of the Paetahi Formation is characterised by a gradual contact with a >10 cm thick paleosol underlying the Kaihouri Tephra (Alloway et al. 1995).

Physical properties of the Poto and Paetahi tephras

Grain size

The majority of the Poto and Paetahi fall layers consist of very coarse ash with variations in grain size ranging from fine ash to coarse lapilli (Tables 1 and 2). The two multi-phase events of the Paetahi Formation are coarser-grained not confined within a clay rich paleosol which produced similar depositional characteristics, each consisting of three events starting with an unconsolidated orange coarse ash to lapilli-dominated layer followed by a change to a finer grain size and shift to a slightly more consolidated coarse grey ash layer.

Componentry

Analysis of components (Table 4) was undertaken on samples from the reference sections (Figure 1; locations 1, 5, and 6) to cover the complete stratigraphic record of the Poto and Paetahi Formations. Within the Poto Formation, the majority of tephra beds in the −1.5 and 0.5 phi size fractions are dominated by brown pumice (ranging from 0%–75%) with some being dominated by lithic clasts (0%–87%), e.g. Poto.g and Poto.j (Figure 7). Of the ten

Table 1. Description of the Poto tephras at the Poto reference location (c.f., Figure 1; location 1). Grain-size parameters determined through dry sieving and GradiSTAT analysis (Blott and Pye 2001).

Layer	Maximum Thickness (cm)	Modality	Sorting	Grain Size (mean)	Componentry	Contact	Description
Poto.a	9	Bimodal	Poorly	Very Fine Lapilli	Brown Pumice	Sharp contact at the base overlying 18 cm thick soil. Gradual contact to 9 cm soil above.	An unconsolidated clast-supported deposit within a yellow-brown clay-rich paleosol which is distinctive and forms the base of the Poto Formation. At the base, the grains appear more reddish brown in the field.
Poto.b	5	Unimodal	Moderately	Very Fine Coarse Ash	Grey Lithics	Sharp contact to 9 cm thick soil below. Sharp contact above to the Ngaere DAD.	Unconsolidated dark grey deposit. Some small lapilli present in the layer, mostly ash particles.
Poto.c lower	4	Polymodal	Very Poorly	Very Coarse Ash	Brown Pumice	Irregular contact at base to 4 cm thick soil. Gradual contact above to Poto.c upper.	Slightly consolidated layer which fines upwards, contained within a yellow-brown clay-rich paleosol.
Poto.c upper	3	Unimodal	Poorly	Coarse Ash	Grey Pumice in coarser fraction. Grey Lithics in finer fraction.	Gradual contact below with Poto.c lower. Sharp contact above to 3 cm thick soil.	Layer appears in pockets across the outcrop. Dominated by unconsolidated material. Layer appears to erode more easily than Poto.c lower.
Poto.d	3	Bimodal	Poorly	Coarse Ash	Grey Pumice in coarser fraction. Brown Pumice in finer fraction.	Wavy contact below to 3 cm thick soil. Wavy contact above with 3 cm thick soil.	Unconsolidated material within yellow-brown clay-rich material. The layer appears in pockets across the outcrop.
Poto.e	4	Trimodal	Very Poorly	Fine Ash	Grey Lithics	Gradual contact with 3 cm thick soil below. Gradual contact above with surge deposit.	Unconsolidated fall layer underlying a surge deposit.
Surge deposit	4					Gradual contact above with Rhyolitic Kawakawa-Oruanui tephra.	Dark brown/grey clay-rich material containing light grey flecks of pumice and small pumice grains 1–2 mm. Only present at the Ronald Road field site in small pockets. The Kawakawa-Oruanui tephra is present directly above.
Poto.f	6	Polymodal	Very Poorly	Very Coarse Ash	Brown Pumice	Sharp contact to rhyolitic Kawakawa-Oruanui tephra below. Gradual contact above to 7 cm thick soil.	Orange-brown consolidated clay-rich paleosol containing a range of pumice and lithic clasts. No apparent grading.
Poto.g	3_8	Unimodal	Moderately	Very Coarse Ash	Grey Lithics	Sharp contact below to 7 cm thick soil. Gradual contact above with 1–2 cm thick soil.	Unconsolidated layer which thickens and thins across the outcrop. Layer has eroded out in areas.
Poto.h	4	Polymodal	Very Poorly	Coarse Ash	Grey Lithics	Wavy contact at base to 1–2 cm thick soil. Wavy contact above with 3 cm thick soil.	Orangey grey consolidated clay-rich layer dominated by grey clasts. Clasts range from 1 mm to 1 cm.
Poto.i	4_7	Polymodal	Very Poorly	Very fine Lapilli	Brown Pumice	Wavy contact below with 3 cm thick soil. Sharp contact above to Poto.j.	Yellowish brown clay-rich paleosol layer, containing weathered pumice. There are some bands containing more grey clasts.
Poto.j	3	Trimodal	Poorly	Very Coarse Ash	Grey Lithics	Sharp contact at base to Poto.i. Sharp contact above with Poto.k lower.	Easily eroded unconsolidated layer which contains a band of lighter grey material in the middle. The layer has been eroded out in patches.
Poto.k lower	8	Polymodal	Very Poorly	Very Coarse Ash	White clay material in coarser fraction. Brown Pumice in finer fraction.	Sharp contact below with Poto.j. Sharp contact above with Poto.k upper.	Layer is within a yellow, brown clay-rich material Appears to contain more grey clasts in the field.
Poto.k upper	4	Polymodal	Poorly	Very Fine Lapilli	Brown Pumice	Sharp contact below with Poto.k lower. Gradual contact above to l. lower.	Strongly weathered layer, within a yellowish-brown clay-rich material. This layer contains more brown lapilli than Poto.k lower.
Poto.l lower	5	Trimodal	Very Poorly	Very Coarse Ash	Grey Lithics in coarser fraction. Brown Pumice in finer fraction.	Gradual contacts to Poto.k upper below and Poto.l upper above.	Yellow-brown consolidated clay-rich paleosol layer containing a higher percentage of clasts 0.5–1 cm diameter.
Poto.l upper	7	Trimodal	Poorly	Very Fine Lapilli	Brown Pumice in coarser fraction. Grey Lithics in finer fraction.	Gradual contacts below with Poto.l lower and above with Poto.m.	Yellow-brown consolidated clay-rich layer which is more clast supported than Poto.l lower showing reverse grading.
Poto.m	11	Polymodal	Very Poorly	Very Coarse Ash	Brown Pumice in coarser fraction. Grey lithics in finer fraction.	Gradual contacts below with Poto.m and above with 5 cm soil.	Strongly weathered consolidated clay-rich layer containing soft and easily breakable pumice and a mix of grey and brown clasts.
Poto.n	8	Polymodal	Very Poorly	Very Coarse Ash	Brown Pumice	Gradual contacts below with 5 cm thick soil. and above with 6 cm thick soil.	Yellow-brown consolidated clay-rich paleosol containing pumice and lithic clasts with a band of orange clasts towards the top.
Poto.o	5	Polymodal	Very Poorly	Coarse Ash	Grey Lithics in coarser fraction. Feldspars and Pyroxenes in finer fraction.	Gradual contact below to 6 cm thick soil. Sharp contact above with well-defined dark brown 6 cm thick soil.	Yellow-brown consolidated clay-rich material., containing pumice and lithic clats. Top section of this layer has a darker orange band.

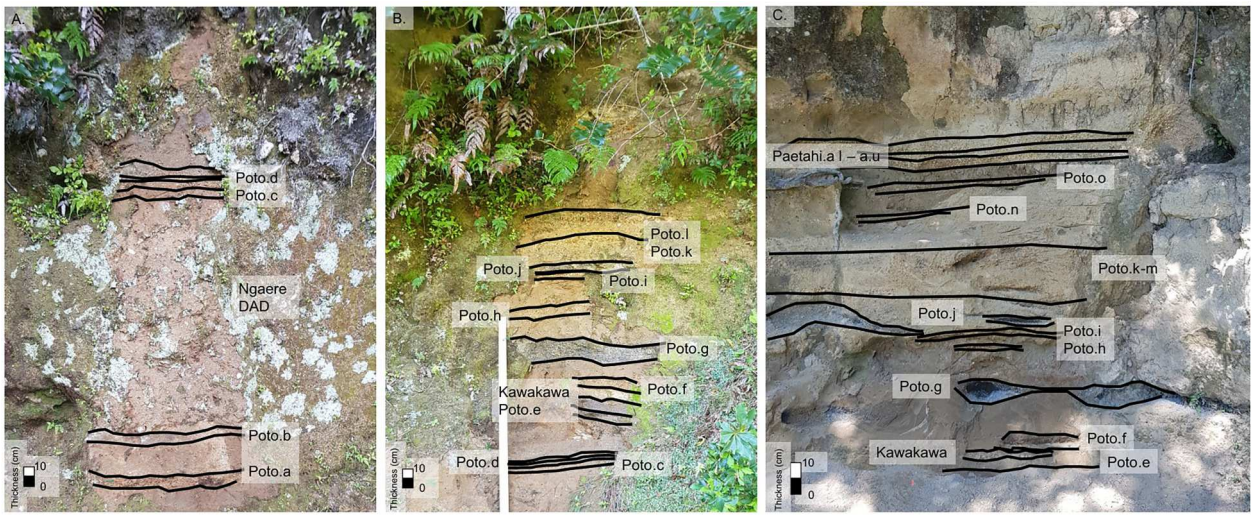

Figure 3. Photos of the Poto Formation at the Poto reference location (1. Opunake Ronald Road) including the Ngaere DAD and the Kawakawa-Oruanui tephra. A. Lower section of Poto.a-Poto.d including the Ngaere DAD, B. Middle section of Ngaere DAD-Poto.l, C. Upper section of Poto.e – Poto.o including the Kawakawa-Oruanui Tephra.

Paetahi tephras the lower and upper layers contain mostly grey lithics (5%–74%) while the more heavily weathered middle layers are rich in brown pumice (5%–50%) (Figure 8). Juvenile-dominated layers within the two formations (Poto.a, cl, cu, d, f, I, ku, ll, lu, m, n and Paetahi.al, am, au, b, d and el) are dominated by either grey (7%–55%) or brown (0%–75%) pumice. Grey lithic clasts show the largest variation in abundance throughout the tephra sequence varying from ~0% to 87% with lithic-rich layers occurring at various stratigraphic levels (Poto.b, e, g, h, j, kl, o and Paetahi.c, em, eu, and f) (Figures 7 and 8). Lithic clasts are dense grey fragments of pre-Poto andesitic lavas (Figure 2) while altered lithics are typically red/orange and sub-angular to sub-rounded dense clasts. Two of the depositional layers contain sedimentary white chalky claystone that breaks easily (7% in Poto.i and 29% in Poto.kl) (Figure 7) and was excavated from the basement during the eruptions with Poto.i being dominated by juveniles whereas Poto.kl is lithic-dominated.

Crystals are predominantly present in the 0.5ϕ size fraction (ranging from 4%–63%) and were rarely found in the −1.5ϕ size fraction (0%–10%). Six stratigraphic layers in the Poto Formation display a larger proportion of crystals in the small size fraction, i.e.

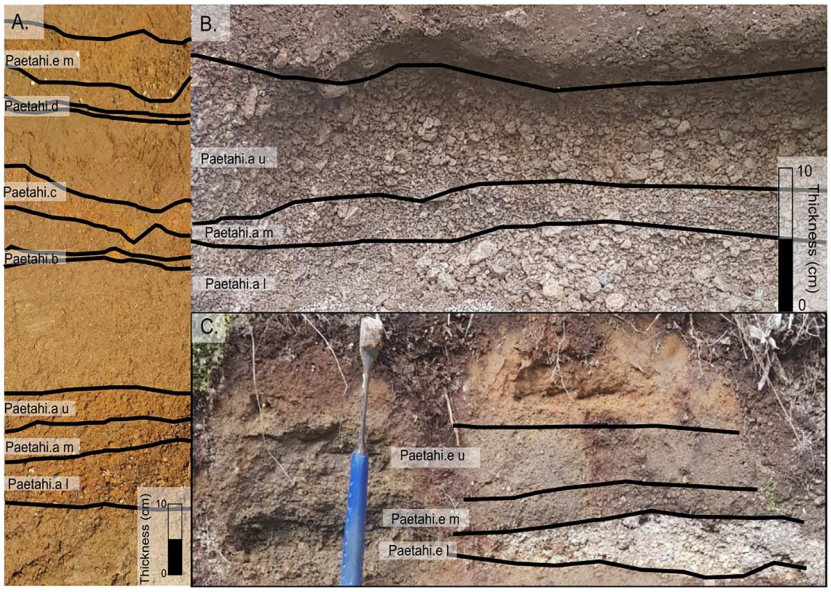

Figure 4. Photos of the Paetahi tephras. A. Depositional sequence of the Paetahi Formation at the Opunake Road reference location (Figure 1; location 5.). B. Close-up image of the Paetahi.a multi-phase sequence showing the internal variation that allowed reclassification into Paetahi.a lower, middle, and upper at the Poto reference location (Figure; location 1. Opunake/ Ronald Road). C. Close-up of the Paetahi.e multi-phase sequence and sub-division into Paetahi.e lower, middle, and upper at the Paetahi Stream reference location (Figure 1; location 6.).

Table 2. Description of the Paetahi tephras at the two Paetahi reference locations (Figure 1; locations 5 and 6). Grain size parameters determined through dry sieving and GradiSTAT analysis (Blott and Pye 2001).

Layer	Maximum Thickness (cm)	Modality	Sorting	Grain Size (mean)	Componentry	Contact	Description
Paetahi.a lower	8	Polymodal	Poorly	Very Coarse Ash	Grey pumice in coarser fraction. Brown Pumice in finer fraction.	Sharp contact below with the 6 cm soil. Gradual contact above with Paetahi.a middle.	Unconsolidated layer, which is the most easily identifiable across the ring plain. Contains lapilli sized pumice and lithics.
Paetahi.a middle	2	Unimodal	Poorly	Very Coarse Ash	Grey Pumice in coarser fraction. Brown Pumice in finer fraction.	Gradual contacts below with Paetahi.a lower and to Paetahi.a upper above.	Slightly consolidated layer. Coarse ash sized grey pumice dominated.
Paetahi.a upper	4	Bimodal	Poorly	Very Fine Lapilli	Brown Pumice	Gradual contact below with Paetahi.a middle. Sharp contact above with 13 cm thick soil.	Unconsolidated layer containing predominantly orange/brown pumice clasts. Very similar to Paetahi.a lower.
Paetahi.b	2	Trimodal	Very Poorly	Coarse Ash	Grey Lithics	Gradual contacts below with 13 cm thick soil and above with 10 cm thick soil.	Strongly weathered layer that appears in pockets across the outcrop within yellow-brown consolidated clay-rich material containing lithics and soft weathered pumice.
Paetahi.c	13	Polymodal	Very Poorly	Medium Ash	Grey Lithics in coarser fraction. Pyroxenes in finer fraction.	Gradual contact below with 10 cm thick soil. Sharp contact above with 8 cm thick soil.	Strongly weathered layer thickens and thins across the outcrop. Occurs within yellow-brown consolidated clay-rich material containing lithics and soft easily erodible pumice.
Paetahi.d	2	Polymodal	Very Poorly	Coarse Ash	Grey Pumice in coarser fraction. Brown Pumice in finer fraction.	Sharp contact below with 8 cm thick soil. Gradual contact above with 6 cm thick soil.	Strongly weathered layer containing soft weathered pumice and lithic clasts within an orange, brown consolidated clay-rich paleosol. Appears in pockets across the deposits.
Paetahi.e lower	7	Trimodal	Poorly	Fine Lapilli	Brown Pumice	Sharp contact below with 6 cm thick soil. Gradual contact above with Paetahi.e middle.	Unconsolidated layer, dominated by very coarse orange lapilli and some grey clasts.
Paetahi.e middle	6	Bimodal	Poorly	Very Coarse Ash	Grey Lithics	Gradual contacts below with Paetahi.e lower below and Paetahi.e upper above.	Slightly consolidated layer, dominated by grey pumice/ lithic clasts within orange, brown clay-rich material.
Paetahi.e upper	9	Trimodal	Very Poorly	Coarse Ash	Grey Lithics in coarser fraction. Grey pumice in finer fraction.	Gradual contact below with Paetahi.e middle. Sharp contact above with Paetahi.f.	Orange, brown clay-rich layer dominated by grey pumice/ lithics. This layer is very well consolidated and very hard.
Paetahi.f	5	Polymodal	Very Poorly	Medium Ash	Grey lithics in coarser fraction. Brown Pumice in finer fraction.	Sharp contact below with Paetahi.f. Gradual contact above with >10 cm thick soil that forms the top of the Paetahi Formation	Strongly weathered layer containing lithics and soft erodible pumice within orange, brown consolidated clay-rich material. The pumice in this layer is very soft and breaks apart easily.

Table 3. Comparison of initial stratigraphic sequence of the Poto and Paetahi Formations from Alloway et al. (1995), with the new stratigraphy refined in this study.

Alloway et al. (1995)	This study
Paetahi.f	Paetahi.f
Paetahi.e	Paetahi.e upper
	Paetahi.e middle
	Paetahi.e lower
Paetahi.d	Paetahi.d
Paetahi.c	Paetahi.c
Paetahi.b	Paetahi.b
Paetahi.a	Paetahi.a upper
	Paetahi.a middle
	Paetahi.a lower
Poto.o	Poto.o
Poto.n	Poto.n
Poto.m	Poto.m
Poto.l	Poto.l upper
	Poto.l lower
Poto.k	Poto.k upper
	Poto.k lower
Poto.j	Poto.j
Poto.i	Poto.i
Poto.h	Poto.h
Poto.g	Poto.g
Poto.f	Poto.f
Kawakawa-Oruanui Tephra	Kawakawa-Oruanui Tephra
Poto.e	Poto.e
Poto.d	Poto.d
Poto.c	Poto.c upper
	Poto.c lower
Ngaere DAD	Ngaere DAD
Poto.b	Poto.b
Poto.a	Poto.a

at the start of the Poto Formation (31%), following the Ngaere DAD (40%), through the middle of the sequence (30%–32%) and at the end of the Poto Formation (63%). There is also a marked increase in crystal abundance towards the middle and upper Paetahi Formation (37%–50%). A higher proportion of free crystals in the small size fraction marks the top units of both formations.

Source eruption parameters

Isopach and isopleth maps for the Poto and Paetahi tephras show elliptical dispersal patterns with aspect ratios ranging from 0.1–0.7 (Figures 9–11; Tables 5 and 6; supplementary material Figure 3–5; Tables 2 and 3). The most widespread fallout deposits are Poto.h, Paetahi.a lower, Paetahi.e lower, and Paetahi.e upper, which have the largest isopach areas of $A^{1/2} = 23.65$, 32.29, 26.88, and 30.31 km^2 respectively. The coarsest layers with the largest areas defined by pumice isopleths are Poto.a, Poto.f, Poto.g, Paetahi.b, and Paetahi.d with $A^{1/2} = 7.75$, 9.58, 7.94, 12.2, and 8.54 km^2 respectively. Poto.b shows the smallest dispersal (isopach $A^{1/2} = 4.94$ km^2), and layers Poto.l upper, Poto.m, Poto.n, Paetahi.a middle and Paetahi.f have the smallest pumice isopleth areas ($A^{1/2} = 5.92$, 5.92, 6.0, 5.1, and 6.0 km^2 respectively). The largest dispersal area for Paetahi.a lower does not come with the coarsest grain size. The thickness of proximal deposits was not available because the older sequences are buried beneath younger material closer to the volcano, leading to a potential underestimation of eruptive volumes with the parameters calculated here representing minimum volumes. Most tephra layers show a similar dispersal direction with main dispersal axes to the east and southeast with some being dispersed to the southwest. The deposits to the southwest need further investigation to allow correlation to the eastern stratigraphy.

Some layers show a dog-leg depositional pattern that trends towards the east before bending southeastwards (e.g. Poto.j and Paetahi.e middle). The dog-leg feature can impact the volume calculations due to the bend in the isopachs affecting the measurements of the long access of dispersal. This feature could be due to preservation of and/or access to the deposits, especially in the south where deposits have been eroded by subsequent activity or covered by tens of metres of younger material. The lack of outcrops of the Poto and Paetahi Formations in the northeast might also be caused by deep burial with younger eruptive products due to this being the dominant wind direction and through industrialisation in this region. However, it could also be the result of different wind directions at different altitudes, i.e. the column reaches a certain height with distance from the vent where after initial deposition to the east a changing wind direction disperses the tephra to the southeast (Sarna-Wojcicki 1981). Models by Weir et al. (2022) for medium to large explosive eruptions from Mt. Taranaki show tephra dispersal across the eastern and southeastern ring plain once the eruption column becomes high enough. The models show a southeastern distribution for M1-3 and L2 eruptions, with L1 and L3 eruptions showing a distribution to the predominant northeast corresponding to mass flow rates of 3×10^6 to 10×10^7 $kg \cdot s^{-1}$ (Weir et al. 2022).

Calculated tephra volumes vary between 0.01 and 0.26 km^3 (Table 5; supplementary material Table 2) with a total volume of 1.6 km^3 for the Poto Formation and 1.4 km^3 for the Paetahi Formation. Paetahi.a lower and Paetahi.e middle have the largest eruptive volumes (0.26 km^3).

Column heights calculated for the individual eruptive events range from 10–20 km, corresponding to subplinian eruptions (Figure 12; Table 7). Mass discharge rates (Q) for the eruptive events are in the order of 10^3 to 10^5 m^3/s, with the corresponding mass eruption rates (MER) ranging from 10^6 to 10^8 kg/s (Table 7). These numbers are minimum values due to the lack of proximal data. The smallest plume height and MER for each formation were observed for the Paetahi.d and Poto.l lower with heights of 9.98 and 10.24 km and MER of 10^6 kg/s 10^6 kg/s, respectively. Paetahi.a lower and Paetahi.e middle have the largest plume heights (19.37 and 19.18 km)

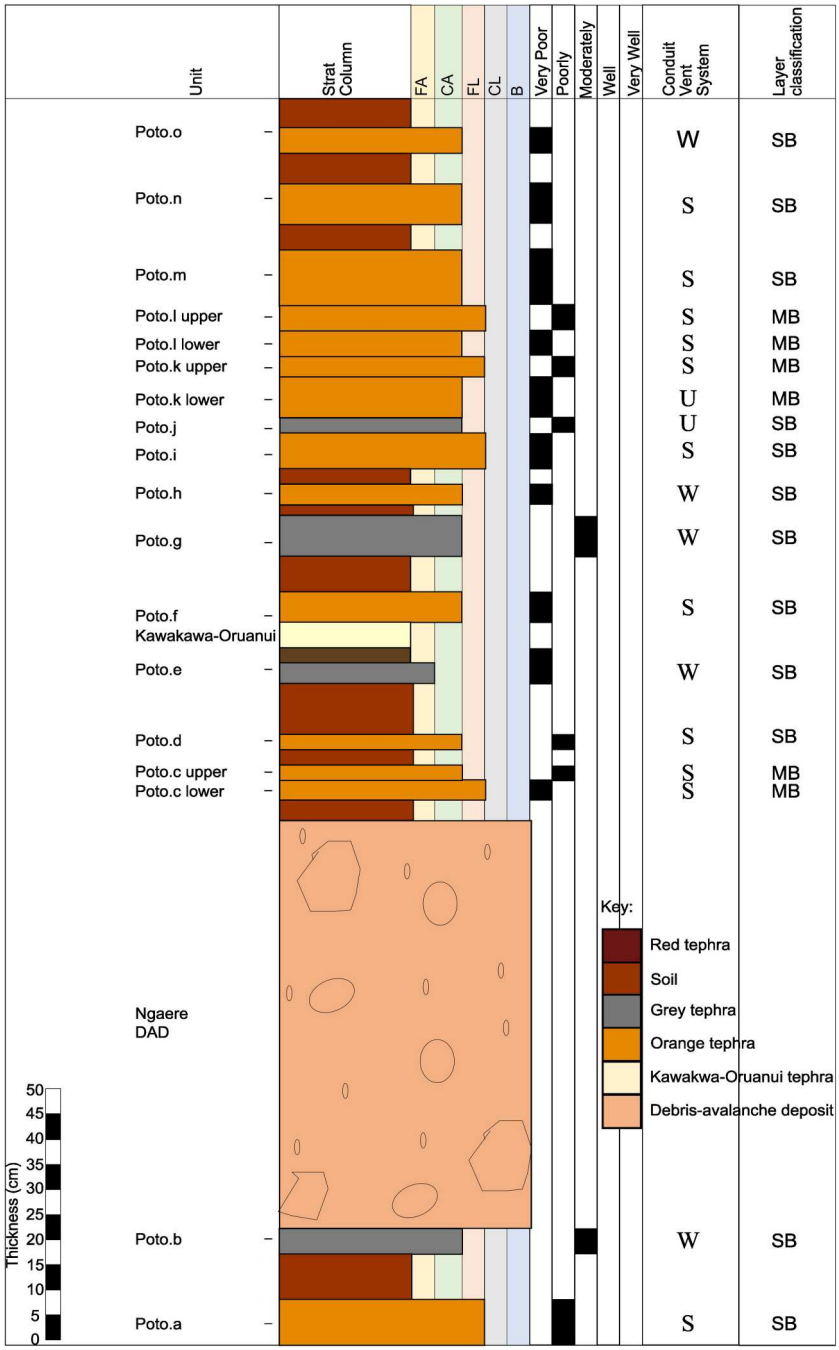

Figure 5. Stratigraphy of the Poto Formation and physical properties, including grain size (FA = fine ash, CA = coarse ash, FL = fine lapilli, and CL = coarse lapilli and B = blocks), sorting, conduit conditions (S = stable conduit system, W = conduit widening and U = unstable column/conduit wall collapse), and eruption classification (MB = multi-phase and SB = single phase eruptive layer). Colours within the stratigraphic column correspond to the colour of the depositional layers in the field. Grain-size classification and sorting (very poorly, poorly, moderately, well, very well) of the deposits determined through dry sieving and GradiSTAT (Blott and Pye 2001).

and MER (10^7 kg/s) of all studied tephras, with Poto.a displaying the largest plume height (18.67 km) and MER (10^7 kg/s) for the Poto Formation. The calculated plume heights and magnitudes between 3 and 4.5 (Figure 12; Table 7) indicate subplinian eruptions with VEIs 3 (moderately large) to 4 (large) (Newhall and Self 1982; Cioni et al. 2015). Estimated minimum duration of individual subplinian events of the Poto and Paetahi Formations range from 1 to 2.5 hours (Figure 13; Table 7).

Interpretations

This study into the stratigraphy and lithosedimentological properties of the Poto and Paetahi Formations provides an in-depth view of eruptive conditions at Mt. Taranaki between 23.1 and 27.30 ka adding to the known <30 ka record. The eruptive period encompassing the Ngaere and Pungarehu collapses was characterised by twenty-eight subplinian eruptive events with similar eruption magnitudes and

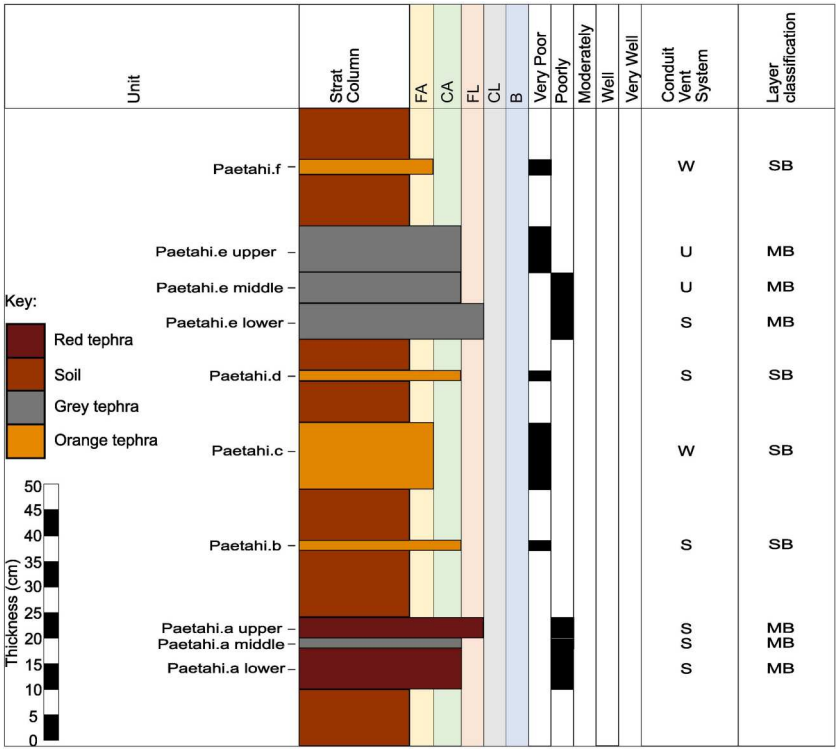

Figure 6. Stratigraphy of the Paetahi Formation and physical properties, including grain size (FA = fine ash, CA = coarse ash, FL = fine lapilli, CL = coarse lapilli and B = blocks), sorting, conduit conditions (S = stable conduit system, W = conduit widening and U = Unstable column/ conduit wall collapse), and eruption classification (MB = multi-phase and SB = single phase eruptive layer). Colours within the stratigraphic columns correspond to the colour of the depositional layers in the field. Grain-size classification and sorting (very poorly, poorly, moderately, well, very well) of the deposits determined through dry sieving and GradiSTAT (Blott and Pye 2001).

conditions recording a high frequency of large explosive events over a 4,000-year interval. This differs from the younger eruptive activity at Mt. Taranaki, which consists of less frequent large explosive eruptions within multi-phase effusive and smaller explosive events. The large eruptions that did occur were predominantly distributed to the northeast differing from the east and southeastern distribution seen for the Poto and Paetahi subplinian events (e.g. Platz et al. 2007; Platz et al. 2012; Torres-Orozco et al. 2017a, 2018; Torres-Orozco et al. 2017b; Lerner et al. 2019a; Lerner et al. 2019c; Cronin et al. 2021). The stratigraphic position of the Poto and Paetahi Formations in relation to the Ngaere and Pungarehu Formations provides a unique opportunity to investigate the impacts of edifice failure on the eruptive processes and size of eruptions at a frequently collapsing stratovolcano. This 4 kyr eruptive period is characterised by two major collapse events (Figure 12; Table 7) that removed large portions of the edifice: 5.85 km^3 as a result of the 27.3 ka Ngaere and 7.5 km^3 during the 24.8 ka Pungarehu collapse (Neall 1979; Alloway et al. 2005; Zernack et al. 2011). The later failure was equivalent to 60% of the present-day volume of the Mt. Taranaki edifice above 1400 m elevation (Zernack et al. 2011; Cronin et al. 2021). Removing such large volumes of material from the upper edifice can significantly influence the post-collapse eruption style depending on the location of the magma source in relation to the upper edifice. The age of the Pungarehu DAD puts the collapse within the period of the Poto and Paetahi Formations (Alloway et al. 2005). The presence of 5 ash fall layers below the Pungarehu DAD within coastal cliff sections of the southwestern ring plain sector further supports the placing of the

Table 4. Description of the components found within the Poto and Paetahi tephra layers.

Lithology	Subgroup	Description
Juveniles	Brown Pumice	Brown to orange pumice clasts which cover a range of densities. Differences in vesicularity were not observable in hand specimen.
	Grey Pumice	Light to dark grey pumice clasts which cover a range of densities. Differences in vesicularity were not observable in hand specimen.
Lithics	Altered Pumice	Brown and grey pumice clasts of previously erupted material which have an orange to white coating over all or part of the clast
	Grey Lithics	Dark grey andesitic lava fragments
	Altered Lithics	Dark grey andesitic lava fragments which have an orange, white coating over all or part of the clast
	White Clay Material	White claystone
Free Crystals	Feldspars	Glassy, white translucent blocky crystal
	Pyroxenes	Dark monoclinic crystals
	Glomerocrysts	Accumulation of crystals

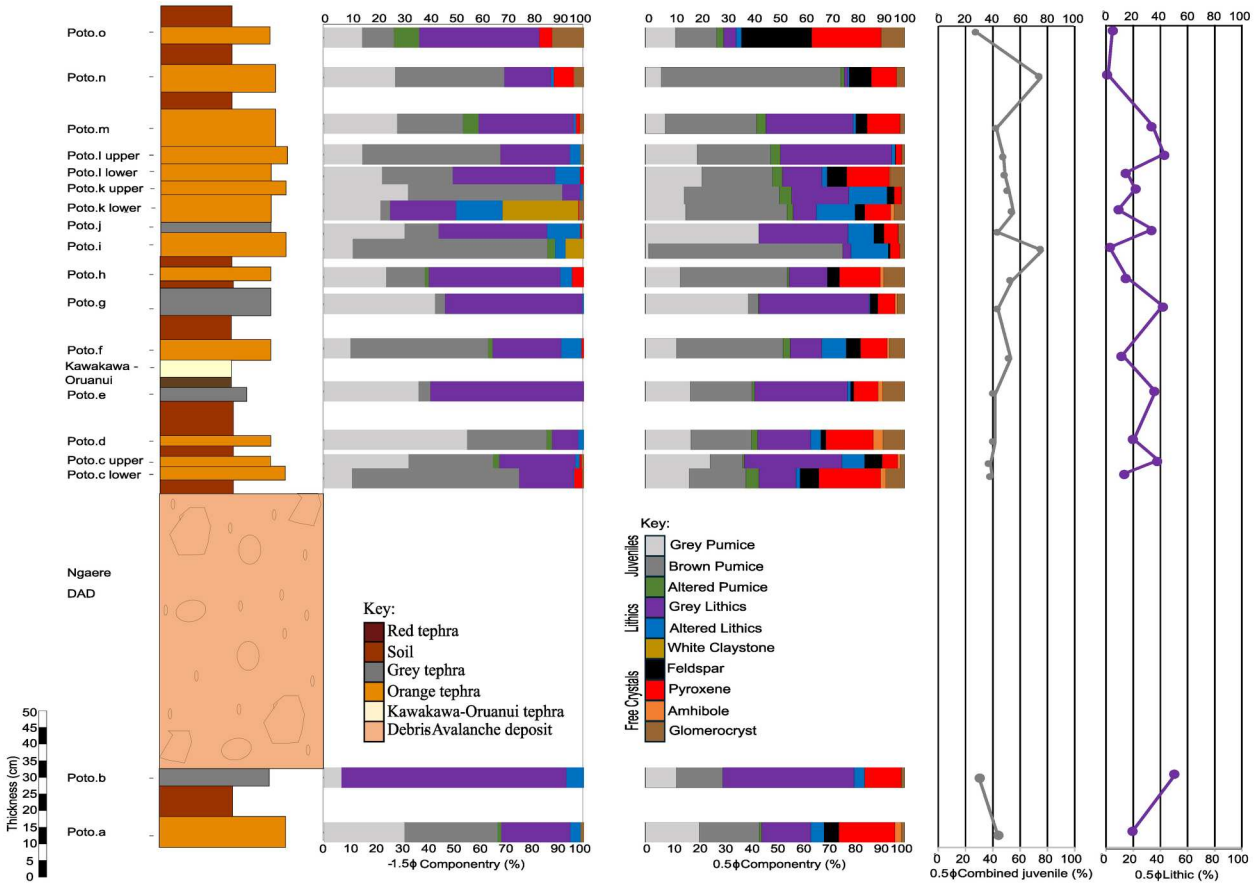

Figure 7. Variation of components making up the −1.5 and 0.5 ϕ size fractions of the Poto tephras in relation to stratigraphy (colours in the stratigraphic column as in Figures 5–6). Line graphs show the combined juvenile and lithic proportions of the analysed clasts from within the 0.5 ϕ size fraction throughout the sequence.

Pungarehu DAD within the eastern stratigraphy (Figure 12).

The proportions of juvenile, lithic, and free crystal components within the different tephra units provide insights into changes in conduit conditions and geometry, which can influence eruption styles (Macedonio et al. 1994; Paredes-Mariño et al. 2019). The dominance of lithics within a fall layer indicates conduit widening, where lithic clasts are ripped off the conduit wall by the rapidly ascending magma

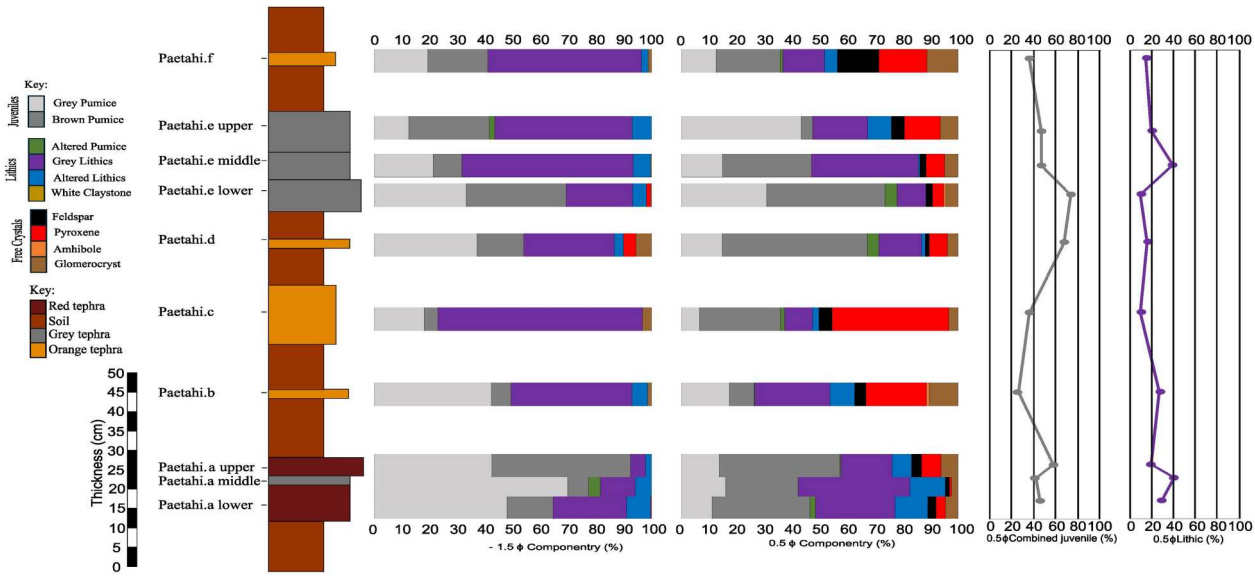

Figure 8. Variation of components making up the −1.5 and 0.5 ϕ size fractions of the Paetahi tephras in relation to stratigraphy (colours in the stratigraphic column as in figures 5–6). Line graphs show the combined juvenile and lithic proportions of the analysed clasts from within the 0.5 ϕ size fraction throughout the sequence.

Table 5. A representative selection of eruptive volumes calculated using AshCalc (Daggitt et al. 2014), using isopachs from the Poto and Paetahi Formations. The remainder of the isopach parameters for the Poto and Paetahi Formations can be found in the supplementary material Table 2.

T (m)	A (Km^2)	A1/2	Perimeter (km)	Shape factor	Long axis	Short axis	Aspect ratio	k	theta	lambda	AshCalc Volume (km^3)
Poto.a								0.9774	0.01208	90.85	0.204
0.1	104.95	10.24	85	0.18	40.62	5.03	0.12				
0.05	340.01	18.44	97	0.45	43.93	13.78	0.31				
Poto.c lower								0.3398	0.004603	76.62	0.1717
0.05	185.03	13.6	83	0.34	39.68	7.54	0.19				
0.03	320.66	17.91	92	0.48	42.26	11.96	0.28				
Paetahi.a lower								0.932	0.01	99.36	0.26
0.1	157.23	12.54	93	0.23	43.43	7.58	0.17				
0.05	419.26	20.48	114.00	0.41	52.02	11.31	0.22				
0.03	1042.52	32.29	138.00	0.69	58.19	23.53	0.40				
Paetahi.a middle								1.13	0.02	41.16	0.06
0.05	131.87	11.48	103.0	0.16	50.10	5.75	0.11				
0.02	550.64	23.47	107	0.60	48.97	14.50	0.30				

(Campbell et al. 2013; Houghton and Carey 2015). Variations in the abundance of lithic clasts throughout an eruptive sequence can indicate pressure changes within the conduit, coupled with a change of depth where fragmentation occurs (Varekamp 1993; Taddeucci and Wohletz 2001). The geometries of the volcanic plumbing, conduit and vent systems control the dynamics of magma ascent and impact the magma supply and discharge rate during an eruption (Scandone and Malone 1985; Bursik 1993; de' Michieli Vitturi et al. 2008; Aravena et al. 2018). Layers dominated by juvenile clasts indicate that magma fragmentation was the dominating process, along with a stable conduit vent system (Taddeucci and Wohletz 2001). The Poto and Paetahi Formations comprise seventeen events characterised by a stable conduit, seven conduit widening events represented by lithic-dominated layers overlying a soil layer that represents a significant break in eruptive activity, and four unstable column/conduit-wall collapse events marked by lithic-dominated layers that follow previous eruptions without a break in time (no soil layer present) (Figures 5 and 6). Within the sequence, only one surge deposit was identified. This thin 4 cm very fine dark brown silty layer was found at the Ronald Road reference section for the Poto Formation directly overlying Poto.e. Poto.i, previously described as a surge deposit (Alloway et al. 1995), is here reclassified as a heavily weathered fall deposit based on its sedimentary features and grain size distribution. This study did not observe any other pyroclastic flow or lahar deposits within the stratigraphic record of these two formations.

Table 6. A representative selection of the isopleth parameters for the Poto and Paetahi Formations. The full set of isopleth parameters can be found within the supplementary data Table 3.

Phi (θ)	A (km^2)	A1/2	Perimeter (km)	Shape factor
Poto.a				
−2.5	415	20.37	86	0.71
−3	112	10.58	47	0.64
−3.5	60	7.75	35	0.62
Poto.c lower				
−0.5	43	6.56	29	0.64
−3.5	45	6.71	35	0.46
Paetahi.a lower				
−2.5	601	24.52	124	0.49
−3	206	14.35	77	0.44
−4	132	11.49	69	0.35
Paetahi.a middle				
−3.5	85	9.22	52	0.4
−4	26	5.1	34	0.28

Fluctuations in the size of the eruptions can be seen throughout the sequence with smaller subplinian events preceding the collapse events (Figure 12; Table 7). Prior to the Ngaere collapse, the conduit was widening, emplacing the Poto.b tephra. While trigger mechanisms for edifice failure at Mt. Taranaki are not well constrained, Alloway et al.(2005) postulated a Bezymianny-type failure for the Ngaere event due to the close stratigraphic relationship of the DAD with the underlying Poto.b. This type of mechanism has been observed at other volcanoes around the globe, e.g. at Mt. St. Helens (Druitt 1992; Belousov et al. 2007), and Bezymianny (Belousov et al. 2007) (Siebert et al. 1987; Vallance et al. 1995; Girina 2013; Pallister et al. 2017). Eruptive activity prior to the Pungarehu failure is characterised by stable conduit conditions, making it difficult to determine the collapse trigger. While a direct relationship with explosive activity or magma intrusion is not indicated by the tephrastratigraphy other likely trigger mechanisms include seismically induced or gravitational, collapse (Alloway et al. 2005; Zernack et al. 2009; Zernack and Procter 2021).

Discussion

Eruption parameters and uncertainties

Previous analysis of eruptive activity from Mt. Taranaki has predominantly focussed on Holocene events, primarily due to the limited preservation of and access to older material. Studies of primary successions have mostly involved deposits that have contributed to the construction of the present-day edifice. However, this

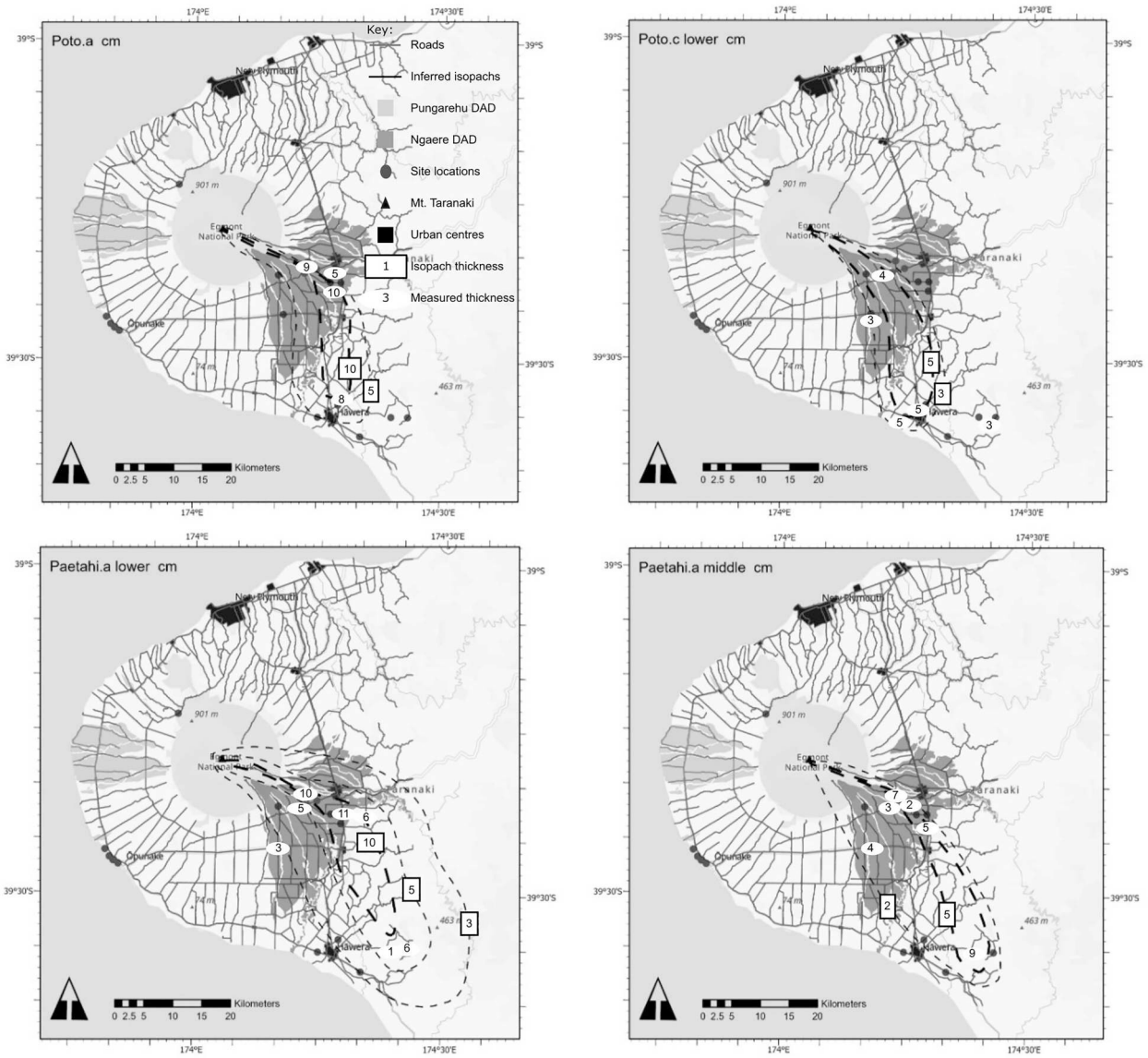

Figure 9. Representative isopach maps for selected Poto and Paetahi tephras showing their distribution across the Taranaki ring plain. The black dots mark the studied locations. The full set of isopach maps is provided as supplementary material Figure 3. Thickness data for each location and layer is available in the supplementary material Table 1. Road and Topographic data sourced from the LINZ Data Service licensed for reuse under CC by 4.0.

represents only <10 kyr of stratigraphy and a limited range of primary deposits. In contrast, the ring plain preserves deposits extending from present day through to approximately 200 ka (Neall 1979; Neall et al. 1986; Alloway et al. 1995; Alloway et al. 2005; Procter et al. 2009; Zernack et al. 2009; Zernack et al. 2011; Damaschke et al. 2017; Zernack 2021). Deposits older than 20 ka are very rarely studied because they are typically buried under tens to hundreds of metres of younger volcaniclastic material (Zernack et al. 2011) and can also be significantly weathered. Older volcaniclastic sequences (<100 ka) at Mt. Taranaki are exposed along coastal cliffs around the southern and western ring plain due to uplift and coastal erosion (Pillans 1990; Palmer et al. 1991; Zernack et al. 2011; Zernack 2021). While some primary fall deposits are embedded in soil and peat layers within these coastal cliffs (Zernack et al. 2009), these show limited lateral extent due to poor preservation in the mass-flow dominated succession.

The total Poto tephra volume is at least 1.6 km^3 with individual events ranging from 0.01–0.2 km^3, magnitudes between 3 and 4.5 (Table 7) and eruption column heights between 10 and 19 km. The total Paetahi tephra volume is at least 1.4 km^3 with individual events ranging from 0.01–0.26 km^3, magnitudes between 3 and 4.5 (Table 7) and eruption column heights of 9.98–20 km. Our study highlights that Mt. Taranaki can produce multiple magnitude 3–4.5 eruptions at regular intervals within an eruptive period, a much higher frequency of large explosive events than previously recorded within the younger volcanic history (c.f., Alloway et al. 1995; Platz et al. 2007; Platz et al. 2012; Torres-Orozco et al. 2017a, 2018; Torres-Orozco et al. 2017b). Distinct contacts between internally homogenous units indicate that they represent

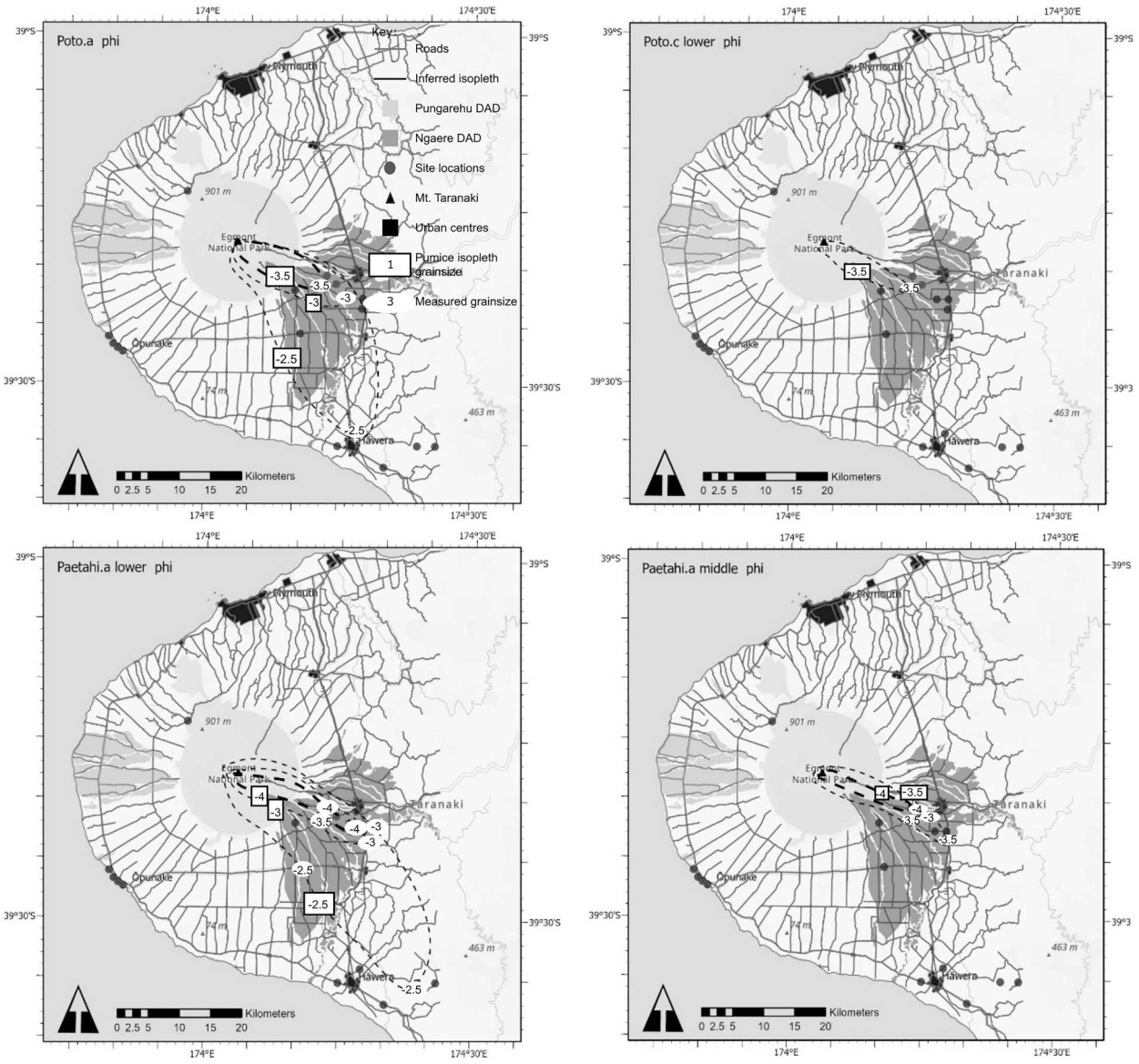

Figure 10. Representative isopleth maps of selected Poto and Paetahi tephras showing their distribution of largest pumice clasts within the layers. Remainder of the isopleth maps for the Poto and Paetahi Formations are within supplementary material Figure 4. Road and Topographic data sourced from the LINZ Data Service licensed for reuse under CC by 4.0.

single-phase events. These single subplinian eruptions were separated from each other by either long or short periods of quiescence, as indicated by intercalated soils or a sharp lithological change between layers, respectively. In contrast, variations in lithosedimentological deposit characteristics suggest that these layers were produced by multi-phase events with internal variations recording changing conditions during the eruption. Due to the age of the Poto and Paetahi Formations, proximal deposits are not accessible or preserved within the stratigraphic record, meaning that smaller eruptive events occurring during this time might have been missed by this study. Younger eruptive records indicate that effusive eruptions coupled with smaller explosive activity were common at Mt. Taranaki (e.g. Platz et al. 2007; Torres-Orozco et al. 2017a; Torres-Orozco et al. 2017b), including directed pyroclastic density currents. The scarcity of such deposits, however, does not exclude the occurrence of smaller eruptive activity during the studied interval but is likely the result of their confinement to the proximal sector of the ring plain (e.g. Torres-Orozco et al. 2017a; Torres-Orozco et al. 2017b; Torres-Orozco et al. 2018; Lerner et al. 2019a; Lerner et al. 2019b; Lerner et al. 2019c), as supported by the presence of a small surge deposit associated with Poto.e.

Poto. a, cl, cu, d, f, I, ku, ll, lu, m, n, Paetahi. al, am, au, b, d and el are dominated by juvenile material (>50% juvenile clasts in the −1. 5θ size fraction) indicating an increased level of magmatic fragmentation (c.f., Taddeucci and Wohletz 2001; Cioni et al. 2015). Stable conduit events are indicated through a higher presence of juvenile clasts as the magma ascends freely through the conduit without excavating the conduit walls (Carey and Houghton 2010; Paredes-Mariño et al. 2019). In contrast, Poto. b, e, g, h, j, kl, o, Paetahi. c, em, eu, and f have lithic contents

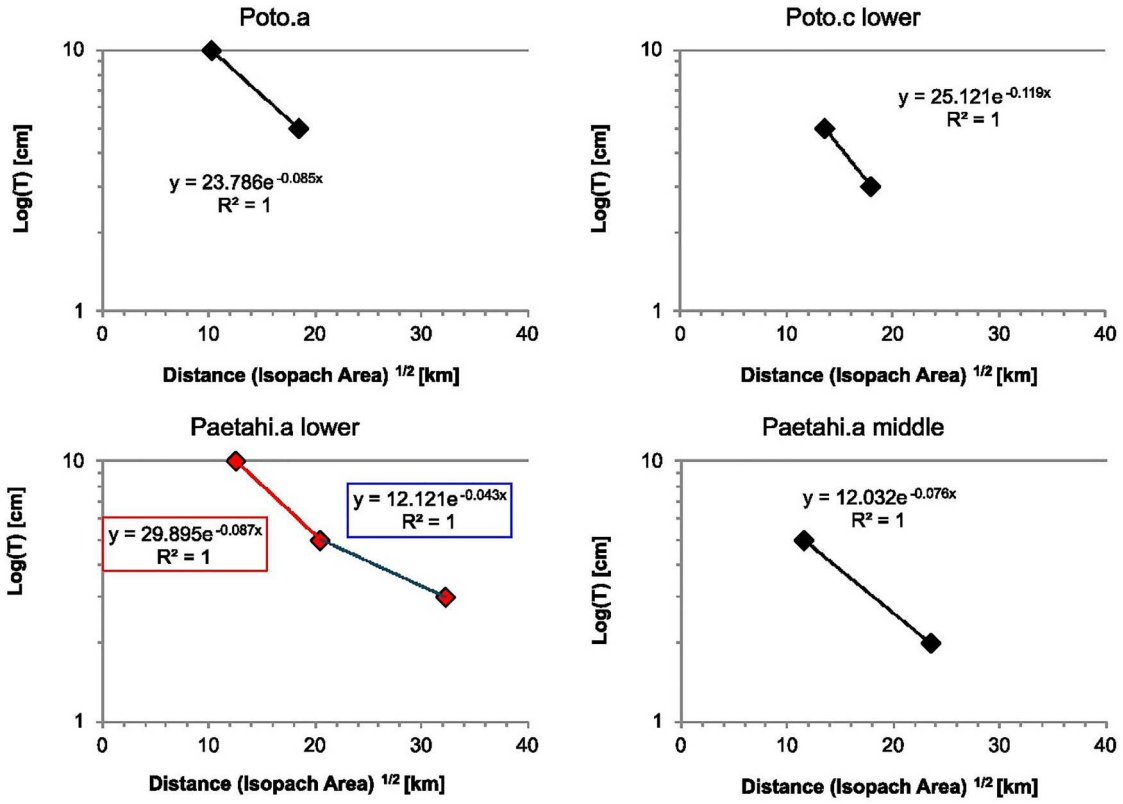

Figure 11. Representative selection of isopach data plots for the individual eruptive layers of the Poto and Paetahi Formations showing one to two segments with different slopes. Colours in Paetahi.a lower show the slopes of the different segments. The full set of isopach data plots can be found as supplementary material Figure 5.

(> 50% in the −1. 5θ size fraction) indicating that the conduit system was experiencing widening or instability, whereas stable conditions are suggested by lithic contents less than 50%. The Lithic contents in the −1. 5θ size fraction were used as the increase in crystal content in the 0.5 θ size fraction subdued the percentages. An increase in the percentage of lithics within multi-phase events as seen in Poto.kl with a lithic increase of 17% and Paetahi. em with a lithic increase of 39% could be related to conduit wall collapse as the mass eruption rate during these eruptions decreased, reducing the height of the eruption column without resulting in a column collapse (Poto.kl 16.1 km, Poto.ku 12.8 km, Paetahi.el 19.2 km, Paetahi.em 19.4 km, and Paetahi.eu 19.1 km) (c.f., Taddeucci and Wohletz 2001; Carey and Houghton 2010; Campbell et al. 2013; Paredes-Mariño et al. 2019). Although conduit wall collapse or widening is evident within several layers (Poto. b, e, g, h, j, kl, o, Paetahi. c, em, eu and f) only Poto.e shows evidence of a column collapse with a thin surge deposit preserved at the reference location (Figure 1; location 1 and Figure 3).

The influence of edifice collapse on pre- and post-eruptive behaviour

A wide range of contributing factors can destabilise a volcanic edifice, including basement tectonics, sloping, gravitational spread, hydrothermal alteration, magmatic intrusion and climatic conditions (Day 1996; McGuire 2003; Lundgren et al. 2004; Albino et al. 2010; Tormey 2010; Roverato et al. 2021). These factors gradually or abruptly weaken the edifice before a trigger mechanism (i.e. magmatic, seismic or climate-/weather-related) generates a collapse (e.g. Gorshkov 1959; Bogoyavlenskaya and Kirsanov 1981; Elsworth and Voight 1995; Elsworth and Voight 1996; Roverato et al. 2021). Three main trigger scenarios have been recognised (Moriya 1980; Siebert et al. 1987). Collapse associated with a magmatic eruption (Bezymianny-type) was first described following the 1957 eruption of Bezymianny Volcano (Kamchatka) and is related to magmatic activity (Gorshkov 1959; Bogoyavlenskaya and Kirsanov 1981). This can be in the form of a magmatic intrusion into the edifice, which was observed in 1980 CE at Mt. St. Helens where the collapse resulted in a lateral blast (Voight et al. 1980; Crandell and Hoblitt 1986; McEwen and Malin 1989; Glicken 1996). Or failure can be triggered by magmatically induced seismicity along with changes in the pore pressure of the rock through mechanical and temperature changes (Voight et al. 1981; Voight et al. 1983; Siebert et al. 1987; Elsworth and Voight 1995; Voight et al. 2002; Zernack and Procter 2021). Other global examples of magmatically induced collapses include Show-Shinzan, Usu-Shinzan (Katsui et al. 1985); and Usu (Minakami et al. 1951). In contrast, Bandai style collapses,

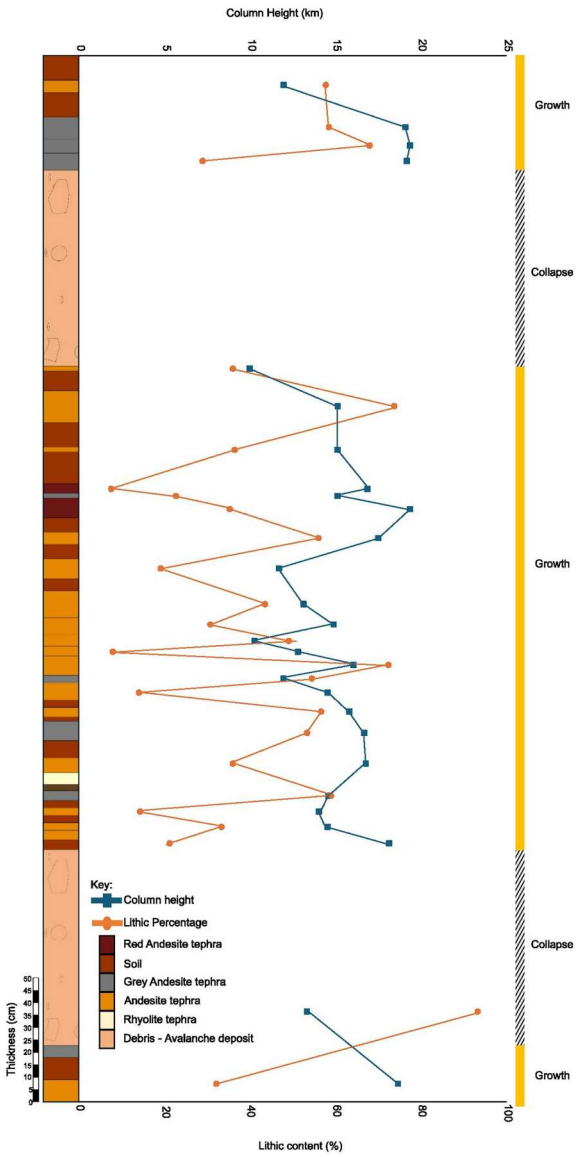

Figure 12. Column height vs. lithic content for all Poto and Paetahi tephras in relation to stratigraphy, highlighting temporal variations in eruption size, lithic proportion and their position within edifice growth and collapse phases.

named after the 1888 CE explosion at Bandai San Volcano (Japan), are triggered by a phreatic eruption without magma being involved. These events are characterised by a lack of juvenile material within the collapse-generated debris avalanche deposit and absence of pyroclastic deposits above or below (Roverato et al. 2021). Tectonic earthquakes can trigger collapse of unstable edifices (Unzen-style) without an eruption occurring as observed in 1792 CE at Unzen Volcano and in 1984 CE at Ontake Volcano (Voight and Elsworth 1997; McGuire 2003).

However, identifying the mechanism that triggered edifice collapse is often impossible (Zernack and Procter 2021), with the exception of several historical cases where it has been constrained, e.g. 1888 CE Bandai; 1956 CE Bezymianny; 1964 CE Shiveluch; 1972 CE Unzen-Mayuyama; 1980 CE Mt. St, Helens, 1984 CE Ontake; and 1997 CE Soufriere Hills (Roverato et al. 2021). Determining what triggered prehistoric or unobserved failures is difficult due to the lack of evidence for potentially preceding seismic or eruptive activity. Pyroclastic deposits directly over- or underlying DADs are not always preserved due to distance from source, erosion and prevailing wind direction (Ponomareva et al. 2006; Sherrod et al. 2007; Zernack et al. 2009; Schaaf and Carrasco-Núñez 2010; Boudon et al. 2013; Watt 2019) and sedimentological features within the produced deposits typically do not record the nature of the trigger either (Zernack and Procter 2021). And while a high proportion of juvenile clasts in DADs could suggest that they were generated during periods of volcanic activity (Zernack et al. 2009; Zernack and Procter 2021), the presence of pumice within DADs is not necessarily evidence for an eruption-induced collapse as large amounts of pumice can be sourced from the surrounding substrate (van Wyk de Vries et al. 2001; Shea et al. 2008; Watt 2019). In addition, even if collapse it not linked to a magmatic intrusion, eruptions can be triggered by a reduction of lithostatic pressure if eruptible magma is present at shallow levels (Watt 2019).

At Mt. Taranaki the trigger mechanism for debris avalanches is unknown except for the Ngaere collapse, which was postulated to be associated with a magmatic eruption (Bezymianny-style collapse) due to its close relationship to the directly underlying Poto.b (Alloway et al. 2005). The remaining collapse events at Mt. Taranaki show no evidence of the trigger mechanism, which could be related to the distance from source where the deposits were observed, their distribution around the volcano in relation to the primary wind direction (north-east) and thus tephra dispersal, and preservation and erosion of encompassing deposits (Zernack et al. 2009). A large proportion of juvenile pumices within the 80–35 ka DADs suggests that these events occurred during an active eruptive period of Mt. Taranaki's history with tectonic events such as large-scale fault movements or gravitational settling-related faulting being the most likely triggers for collapse once a critical edifice height has been reached (Zernack et al. 2009).

In addition, climatic factors such as high-intensity rainstorms can cause a reduction in edifice strength due to saturation (McGuire 2003; Scott et al. 2005; Carrasco-Núñez et al. 2006) and could have initiated smaller failures at Mt. Taranaki (Zernack et al. 2009).

A sudden shift in the lithostatic pressure following a collapse event can influence the eruptive behaviour associated due to depressurisation and unloading impacting the magmatic system below (Pinel and Jaupart 2005; Albino et al. 2010; Pinel and Albino 2013). This has been linked to the relationship between edifice size, magmatic reservoir and collapse volume (Watt 2019; Zernack and Procter 2021). A collapse can cause a change in eruptive style, increased

Table 7. Estimated eruption parameters for the Poto and Paetahi Formations based on the calculated volumes listed in Table 3 through AshCalc (Daggitt et al. 2014), calculated using Pyle (2000) and Mastin et al. (2009). The full dataset is provided as supplementary data Table 2.

Formation	Layer	Column height (H^t) (Mastin et al. 2009)	Volume Discharge m^3/s (Q) (Mastin et al. 2009)	Log10 Mass eruption rate (MER) (kg/s)	Eruptive magnitude (Pyle 2000)	Duration (hours)	Eruption style
Poto	a	18.7	11149.5	7.45	4.31	2.03	Subplinian
	b	13.3	3044.6	6.88	3.51	1.17	Subplinian
	Ngaere DAD						
	c.l	18.2	10046.8	7.4	4.23	1.9	Subplinian
	c.u	14.6	4260.9	7.03	3.69	1.28	Subplinian
	d	14.0	3710.5	6.97	3.61	1.23	Subplinian
	e	14.6	4333.9	7.03	3.70	1.28	Subplinian
	f	16.8	7425.8	7.27	4.03	1.6	Subplinian
	g	16.7	7253.9	7.26	4.01	1.58	Subplinian
	h	15.8	5875.9	7.17	3.88	1.43	Subplinian
	i	14.6	4270.9	7.03	3.69	1.28	Subplinian
	j	11.9	1984.2	6.70	3.30	1.11	Subplinian
	k.l	16.1	6260.1	7.19	3.92	1.47	Subplinian
	k.u	12.8	2614.5	6.82	3.43	1.14	Subplinian
	l.l	10.2	1097.5	6.44	3.04	1.11	Subplinian
	l.u	14.9	4669.6	7.07	3.74	1.31	Subplinian
	m	13.1	2867.3	6.86	3.48	1.16	Subplinian
	n	11.7	1827.6	6.66	3.26	1.10	Subplinian
	o	17.5	8723.3	7.34	4.14	1.74	Subplinian
Paetahi	a.l	19.4	12850.0	7.51	4.41	2.25	Subplinian
	a.m	15.1	4967.2	7.09	3.78	1.34	Subplinian
	a.u	16.9	7572.1	7.28	4.04	1.61	Subplinian
	b	15.1	4967.2	7.09	3.78	1.34	Subplinian
	c	15.1	4967.2	7.09	3.78	1.34	Subplinian
	d	10.0	992.1	6.39	3	1.12	Subplinian
	Pungarehu DAD						
	e.l	19.2	12369.7	7.49	4.39	2.19	Subplinian
	e.m	19.4	12850.0	7.51	4.41	2.25	Subplinian
	e.l	19.1	12179.5	7.48	4.37	2.16	Subplinian
	f	12.0	2007.6	6.70	3.30	1.11	Subplinian

eruption rate (frequency and/or magnitude), or a shift towards a more mafic composition (c.f., Siebert et al. 2004; Tibaldi 2004; Hora et al. 2009; Manconi et al. 2009; Watt 2019), although some volcanoes display no apparent change in eruptive behaviour (Ponomareva et al. 2006; Zernack et al. 2012; Zernack and Procter 2021). Post-collapse changes in eruptive styles have been observed globally, for example, a shift from dome-forming activity to explosive eruptions at Pelée, Martinique (Boudon et al. 2013; Germa et al. 2015; Watt 2019). Large explosive events triggered by collapse were followed by effusive activity at Mt. St. Helens in 1980 CE (Glicken 1996), Bezymianny in 1956 CE (Belousov et al. 2007), and Augustine in 1883 CE (Siebert et al. 1987; Watt 2019). The post-collapse effusive dome-building stage at these volcanoes began to fill in the collapse scars (Watt 2019). The response of the magmatic system following edifice

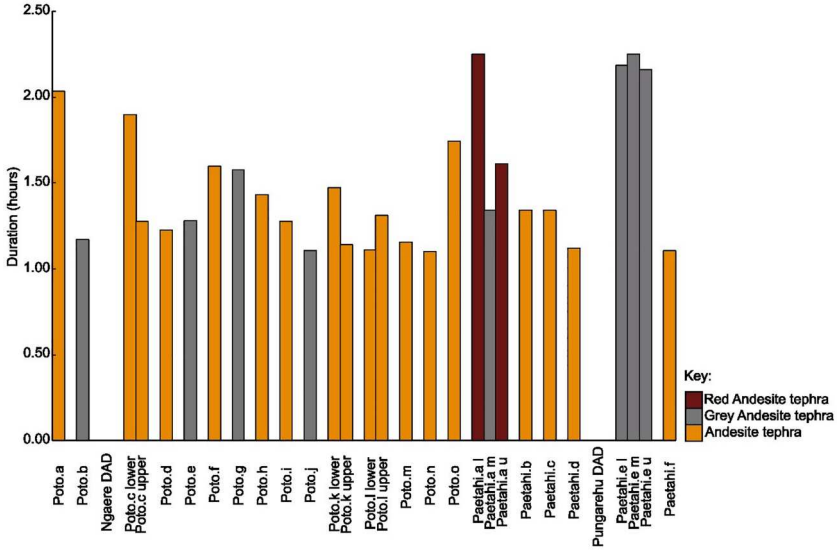

Figure 13. Histogram showing the calculated duration of eruptions that produced the Poto and Paetahi tephras. Colours relate to the stratigraphic colours in Figure 12.

collapse is confined to the mid-upper crustal system (Watt 2019).

Apart from Mt. Taranaki, many volcanoes globally have experienced multiple collapse events throughout their eruptive history, e.g. Mt. Rainier (6) (Crandell 1971; Scott et al. 1995; Vallance and Scott 1997); Mt. St. Helens (4) (Hausback and Swanson 1990; Glicken 1996); and Mt. Ruapehu (10) (Keigler et al. 2011; Tost et al. 2014; Tost and Cronin 2016). Collapses are followed by periods of regrowth resulting in DADs being intercalated with primary and secondary deposits across the volcanic ring plains (Zernack et al. 2011; Zernack and Procter 2021). The recurrence rate of debris avalanches is related to the magma supply rate of a volcano and can range from 0.1–1 kyr for frequent small collapse (>1 km^3) typical for small dome collapse edifices, and 1–10 kyr for small to large failures (<1 km^3) at stratovolcanoes and to 10–100 kyr for the largest observed collapses (>20–5,000 km^3) observed at ocean island volcanoes (Zernack and Procter 2021 and references therein) Mt. Taranaki has experienced at least fourteen collapse events since 200 ka with volumes ranging from 1–7.5 km^3 and a recurrence rate of 8–9 kyr corresponding to a magma supply rate of 0.45 km^3/kyr (Zernack et al. 2012b; Zernack and Procter 2021). Observed high recurrence rates at Shiveluch and Mt. St. Augustine (600–2,000 years and 150–300 years) is related to a high magma supply rate of 15 km^3/kyr and 1–3 km^3/kyr respectively and small collapse size (1–2.5 km^3 and 0.2–0.5 km^3 respectively). In comparison Mt. Taranaki has experienced much larger edifice collapse events with the Ngaere and Pungarehu corresponding to approximately 60% of the edifice volume above 1400 m being removed (Zemeny et al. 2023).

However, the short recurrence time and large magnitude of the Ngaere and Pungarehu is unusual in a global context as a repose time of c. 2,500 years between failures appears to be too short to fully rebuild the edifice after the first collapse. A likely explanation for two large failures occurring in close succession is that they involved different portions of the same paleo-edifice, which is supported by the dispersal of the resulting debris-avalanche deposits in opposite directions, the Ngaere to the east followed by the Pungarehu to the west. The second collapse although larger removed the remnant cone and did not involve the material directly above the vent. This is reflected in the Poto and Paetahi tephras where the magmatic system was impacted following the Ngaere but not the Pungarehu collapse.

Post- Ngaere, the Poto and Paetahi Formations record a higher frequency of large explosive events than recorded in the younger eruptive succession (c.f., Neall 1972; Alloway et al. 1995; Platz et al. 2007; Damaschke et al. 2017; Torres-Orozco et al. 2017a; Torres-Orozco et al. 2017b). Open conduit conditions following both collapse events allowed magma to move freely through the system. This was accompanied by increased eruption column heights of 18.18 km (Poto.c lower post-Ngaere) and 19.18 km (Paetahi.e lower post-Pungarehu) compared to pre-failure heights of 13.34 km (Poto.b) and 9.98 km (Paetahi.d). Such an increase in the frequency of large explosive events has also been observed at Shiveluch, Kamchatka (Belousov et al. 1999; Gorbach et al. 2013) and Mt. Pelée, Martinique (32 ka) (Boudon et al. 2013; Germa et al. 2015).

Implications for future eruption scenarios and hazard modelling

Globally, pre-Holocene volcanic deposits are underrepresented within stratigraphic studies due to poor preservation or subsequent burial. Hazard modelling and mitigation plans for Mt. Taranaki are typically based on eruption styles and frequency known for the well-studied <5 ka volcanic history (e.g. McDonald et al. 2017; Torres-Orozco et al. 2018; Weir et al. 2022). This short eruptive record fails to account for hazards associated with morphological changes caused by small to large edifice collapse events, with the last failure occurring at 7.5 ka. Our study highlights the importance of including long-term volcanic records to generate more accurate hazard models for long-lived stratovolcanoes that experience frequent edifice collapse, with the Poto and Paetahi Formations providing the unique opportunity to investigate the volcanic response to repeated collapse and regrowth.

Furthermore, this 4 kyr eruptive period 23.1–27.3 ka, experienced a larger number of major explosive eruptions with eruption columns reaching heights of c. 10–20 km (Bebbington and Jenkins 2019). This contrasts the eruptive hazard forecasting for Mt. Taranaki, which is based on the younger record characterised by a lower frequency of major explosive eruptions, and a wider range of eruptive styles e.g. effusive to large explosive (Torres-Orozco et al. 2017a, 2018; Torres-Orozco et al. 2017b; Bebbington and Jenkins 2019; Weir et al. 2022). Within the last 5,000 years, sixteen subplinian to plinian eruptions have been recorded (column heights14–29 km; and magnitudes of 4.1–5.1), with the last occurring in 1655 CE (Platz et al. 2007; Torres-Orozco et al. 2018). This indicates that the higher frequency of large explosive eruptions during the Poto and Paetahi eruptive periods could be a response to the collapse-induced morphological changes of the edifice, which generated an open system that allows magma to freely ascend to the surface without stalling.

Furthermore, the dispersal of the Poto and Paetahi tephras across the southeastern ring plain differs from the predominant northeastern distribution seen for <5 ka tephras (Torres-Orozco et al. 2017a, 2018; Torres-

Orozco et al. 2017b). This finding is supported by modelling, which shows that eruptions of a certain size produce tephra dispersal across the southeastern sector of the ring plain (Weir et al. 2022). Thus, our study highlights the limitations of using only Holocene records for risk assessments, as this short interval might not fully capture how eruptive styles and the dispersal of eruptives may be changing over longer time scales or in response to external factors.

Conclusions

Investigating a sequence of eruptions that comprises two major edifice collapses exposed the complexity of long-term volcanic processes at an andesite stratovolcano and their role in eruption behaviour. Our revised stratigraphy for the Poto and Paetahi Formations shows that this period in Mt. Taranaki's history was marked by increased explosive activity that produced twenty-eight subplinian events and one pyroclastic surge deposit. These tephra formations differ from previously studied younger eruptive periods, which show a wider array of eruptive styles and less frequent large explosive events. The 4 kyr Poto and Paetahi eruptive periods were characterised by frequent and consistently large explosive events with a total eruptive volume of 3 km^3 and 0.01–0.26 km^3 of tephra produced during individual eruptive events. Eruption column heights ranged from 10–20 km with eruption magnitudes of 3–4.5 VEI. Post-collapse eruptions were larger than pre-failure events with eruption sizes varying during edifice growth between the two collapse events. Throughout this period of increased large explosive eruptions, changes in componentry between layers indicate varying conduit conditions with seventeen units being classified as stable conduit events, seven as conduit widening events, and four as unstable column/conduit wall collapse events.

The dispersal of the studied tephras to the east and southeast differs from younger deposits at Mt. Taranaki, with some additional layers identified along the southwestern coastline that fall within the same period. However, further work is required to integrate these into the stratigraphy. While the distribution of the Poto and Paetahi tephras diverges from the predominant northeasterly distribution of younger tephras due to the prevailing westerly wind direction, it supports tephra fall models for the area which show eruptions of a certain size being distributed to the southeast. Thus, our results have significant implications for future volcanic risk assessment in the Taranaki region and should be taken into account for developing future hazard scenarios.

The relationship between collapse volume and total volume of the edifice appears to play a role for the size of post-failure eruptions and potential changes or lack of changes seen in subsequent eruptive styles. The Pungarehu and Ngaere DADs both represent a significant percentage of the cone (up to approximately 60%) being removed, depressurising the system, and resulting in a 4,000 year-long period of heightened explosive activity at Mt. Taranaki. The concept of large edifice collapses leading to an increase in large eruptive events without changing eruptive styles might apply to repeatedly collapsing stratovolcanoes elsewhere. Understanding how eruptive behaviour may change not only due to magmatic processes but external influences is critical for hazard forecasting and planning. Thus, these collapse events and the generation of the Poto and Paetahi tephra formations highlight the need to extend eruptive histories for hazard modelling at volcanoes around the world to include longer-term records.

Acknowledgements

We are grateful to the Taranaki Farmers that allowed access to their land and also thank Shane Cronin for his support in the field. The anonymous reviewers are thanked for their comments on the manuscript.

Disclosure statement

No potential conflict of interest was reported by the author(s).

Funding

This research was supported financially by the MBIE Endeavour Fund Research Program 'Transitioning Taranaki to a Volcanic Future' – UOAX1913, and the Resilience to Nature's Challenges Volcano program - GNS-RNC047. SM was supported by a Massey University Doctoral Scholarship, and the Dr Eileen Fair Earth Science Doctoral Scholarship.

Data availability statement

The data that support the findings of this study are openly available in zenodo at https://zenodo.org/records/14454156.

ORCID

Shannen Mills http://orcid.org/0009-0006-2301-2567
Jonathan Procter http://orcid.org/0000-0001-8271-1137
Anke Zernack http://orcid.org/0000-0002-5771-7286
Stuart Mead http://orcid.org/0000-0003-3135-439X

References

Albino F, Pinel V, Sigmundsson F. 2010. Influence of surface load variations on eruption likelihood: application to two Icelandic subglacial volcanoes, Grímsvötn and Katla. Geophysical Journal International. 181(3):1510–1524. doi:10.1111/j.1365-246X.2010.04603.x.

Alloway B, McComb P, Neall V, Vucetich C, Gibb J, Sherburn S, Stirling M. 2005. Stratigraphy, age, and correlation of voluminous debris-avalanche events from an ancestral Egmont volcano: implications for coastal plain

construction and regional hazard assessment. Journal of the Royal Society of New Zealand. 35(1-2):229–267. doi:10.1080/03014223.2005.9517782.

Alloway B, Neall VE, Vucetich CG. 1995. Late Quaternary (post 28,000 year B.P.) tephrostratigraphy of northeast and central Taranaki, New Zealand. Journal of the Royal Society of New Zealand. 25(4):385–458. doi:10.1080/03014223.1995.9517496.

Aravena Á, Cioni R, de'Michieli Vitturi M, Neri A. 2018. Conduit stability effects on intensity and steadiness of explosive eruptions. Scientific Reports. 8(1):4125. doi:10.1038/s41598-018-22539-8.

Bebbington MS, Jenkins SF. 2019. Intra-eruption forecasting. Bulletin of Volcanology. 81(6):34. doi:10.1007/s00445-019-1294-9.

Belousov A, Belousova M, Voight B. 1999. Multiple edifice failures, debris avalanches and associated eruptions in the Holocene history of Shiveluch volcano, Kamchatka, Russia. Bulletin of Volcanology. 61(5):324–342. doi:10.1007/s004450050300.

Belousov A, Voight B, Belousova M. 2007. Directed blasts and blast-generated pyroclastic density currents: a comparison of the Bezymianny 1956, Mount St Helens 1980, and Soufrière Hills, Montserrat 1997 eruptions and deposits. Bulletin of Volcanology. 69(7):701–740. doi:10.1007/s00445-006-0109-y.

Belousov AB. 1995. The Shiveluch volcanic eruption of 12 November 1964—explosive eruption provoked by failure of the edifice. Journal of Volcanology and Geothermal Research. 66(1):357–365. doi:10.1016/0377-0273(94)00072-O.

Blott SJ, Pye K. 2001. GRADISTAT: a grain size distribution and statistics package for the analysis of unconsolidated sediments. Earth Surface Processes and Landforms. 26(11):1237–1248.

Bogoyavlenskaya G, Kirsanov I. 1981. Twenty five years of volcanic activity of Bezymianny. Volcanol Seismol. 2:3–13.

Bonadonna C, Costa A. 2012. Estimating the volume of tephra deposits: a new simple strategy. Geology. 40(5):415–418. doi:10.1130/g32769.1.

Bonadonna C, Costa A. 2013. Plume height, volume, and classification of explosive volcanic eruptions based on the Weibull function. Bulletin of Volcanology. 75(8):742. doi:10.1007/s00445-013-0742-1.

Bonadonna C, Ernst GGJ, Sparks RSJ. 1998. Thickness variations and volume estimates of tephra fall deposits: the importance of particle Reynolds number. Journal of Volcanology and Geothermal Research. 81(3):173–187. doi:10.1016/S0377-0273(98)00007-9.

Bonadonna C, Houghton BF. 2005. Total grain-size distribution and volume of tephra-fall deposits. Bulletin of Volcanology. 67(5):441–456. doi:10.1007/s00445-004-0386-2.

Boudon G, Villemant B, Friant AL, Paterne M, Cortijo E. 2013. Role of large flank-collapse events on magma evolution of volcanoes. Insights from the Lesser Antilles Arc. Journal of Volcanology and Geothermal Research. 263:224–237. doi:10.1016/j.jvolgeores.2013.03.009.

Bursik M. 1993. Subplinian eruption mechanisms inferred from volatile and clast dispersal data. Journal of Volcanology and Geothermal Research. 57(1):57–70. doi:10.1016/0377-0273(93)90031-L.

Campbell ME, Russell JK, Porritt LA. 2013. Thermomechanical milling of accessory lithics in volcanic conduits. Earth and planetary science letters. 377-378:276–286. doi:10.1016/j.epsl.2013.07.008.

Capra L, Macías JL. 2002. The cohesive Naranjo debris-flow deposit (10 km^3): a dam breakout flow derived from the Pleistocene debris-avalanche deposit of Nevado de Colima Volcano (México). Journal of Volcanology and Geothermal Research. 117(1):213–235. doi:10.1016/S0377-0273(02)00245-7.

Carey RJ, Houghton BF. 2010. "Inheritance": an influence on the particle size of pyroclastic deposits. Geology. 38(4):347–350. doi:10.1130/g30573.1.

Carey S, Sigurdsson H. 1985. The May 18, 1980 eruption of Mount St. Helens: 2. Modeling of dynamics of the Plinian Phase. Journal of Geophysical Research. 90:2948–2958. doi:10.1029/JB090iB04p02948.

Carey S, Sparks RSJ. 1986. Quantitative models of the fallout and dispersal of tephra from volcanic eruption columns. Bulletin of Volcanology. 48(2):109–125. doi:10.1007/BF01046546.

Carrasco-Núñez G, Díaz-Castellón R, Siebert L, Hubbard B, Sheridan MF, Rodríguez SR. 2006. Multiple edifice-collapse events in the Eastern Mexican Volcanic Belt: the role of sloping substrate and implications for hazard assessment. Journal of Volcanology and Geothermal Research. 158(1):151–176. doi:10.1016/j.jvolgeores.2006.04.025.

Cas RAF, Wright JV. 1987. Volcanic successions modern and ancient. Volcanic successions: modern and ancient. doi:10.1007/978-94-009-3167-1.

Cioni R, Pistolesi M, Rosi M. 2015. Plinian and subplinian eruptions. In: Sigurdsson H, editor. The encyclopedia of volcanoes (second edition). San Diego (CA): Academic Press; p. 519–535. doi:10.1016/B978-0-12-385938-9.00029-8.

Cole PD, Queiroz G, Wallenstein N, Gaspar JL, Duncan AM, Guest JE. 1995. An historic subplinian/phreatomagmatic eruption: the 1630 AD eruption of Furnas volcano, São Miguel, Azores. Journal of Volcanology and Geothermal Research. 69(1):117–135. doi:10.1016/0377-0273(95)00033-X.

Crandell DR. 1971. Postglacial lahars from Mount Rainier volcano, Washington. Professional Paper.

Crandell DR, Hoblitt RP. 1986. Lateral blasts at Mount St. Helens and hazard zonation. Bulletin of Volcanology. 48(1):27–37. doi:10.1007/BF01073511.

Cronin SJ, Zernack AV, Ukstins IA, Turner MB, Torres-Orozco R, Stewart RB, Smith IEM, Procter JN, Price R, Platz T, et al. 2021. The geological history and hazards of a long-lived stratovolcano, Mt. Taranaki, New Zealand. New Zealand Journal of Geology and Geophysics. 64(2-3):456–478. doi:10.1080/00288306.2021.1895231.

Daggitt ML, Mather TA, Pyle DM, Page S. 2014. AshCalc–a new tool for the comparison of the exponential, power-law and Weibull models of tephra deposition. Journal of Applied Volcanology. 3(1):7. doi:10.1186/2191-5040-3-7.

Damaschke M, Cronin SJ, Holt KA, Bebbington MS, Hogg AG. 2017. A 30,000 yr high-precision eruption history for the andesitic Mt. Taranaki, North Island, New Zealand. Quaternary Research. 87:1–23. doi:10.1017/qua.2016.11.

Day S. 1996. Hydrothermal pore fluid pressure and the stability of porous, permeable volcanoes. Geological Society, London, Special Publications. 110(1):77–93.

Day S, Llanes P, Silver E, Hoffmann G, Ward S, Driscoll N. 2015. Submarine landslide deposits of the historical lateral collapse of Ritter Island, Papua New Guinea. Marine and Petroleum Geology. 67:419–438. doi:10.1016/j.marpetgeo.2015.05.017.

de' Michieli Vitturi M, Clarke AB, Neri A, Voight B. 2008. Effects of conduit geometry on magma ascent dynamics in dome-forming eruptions. Earth and Planetary Science Letters. 272(3):567–578. doi:10.1016/j.epsl.2008.05.025.

de Silva SL, Davidson JP, Croudace IW, Escobar A. 1993. Volcanological and petrological evolution of Volcan Tata Sabaya, SW Bolivia. Journal of Volcanology and Geothermal Research. 55(3):305–335. doi:10.1016/0377-0273(93)90043-Q.

Druitt TH. 1992. Emplacement of the 18 May 1980 lateral blast deposit ENE of Mount St. Helens, Washington. Bulletin of Volcanology. 54(7):554–572. doi:10.1007/BF00569940.

Elsworth D, Voight B. 1995. Dike intrusion as a trigger for large earthquakes and the failure of volcano flanks. Journal of Geophysical Research: Solid Earth. 100(B4):6005–6024.

Elsworth D, Voight B. 1996. Evaluation of volcano flank instability triggered by dyke intrusion. Geological Society, London, Special Publications. 110(1):45–53.

Fierstein J, Nathenson M. 1992. Another look at the calculation of fallout tephra volumes. Bulletin of Volcanology. 54(2):156–167. doi:10.1007/BF00278005.

Fisher RV, Schmincke H-U. 1984. Pyroclastic rocks and tectonic environment. In: Fisher RV, Schmincke H-U, editors. Pyroclastic rocks. Berlin Heidelberg: Springer; p. 383–409. doi:10.1007/978-3-642-74864-6_14.

Folk RL, Ward WC. 1957. Brazos River bar [Texas]; a study in the significance of grain size parameters. Journal of Sedimentary Research. 27(1):3–26. doi:10.1306/74d70646-2b21-11d7-8648000102c1865d.

Germa A, Lahitte P, Quidelleur X. 2015. Construction and destruction of Mont Pelée volcano: volumes and rates constrained from a geomorphological model of evolution. Journal of Geophysical Research (Earth Surface). 120:1206–1226. doi:10.1002/2014jf003355.

Germa A, Quidelleur X, Lahitte P, Labanieh S, Chauvel C. 2011. The K–Ar Cassignol–Gillot technique applied to western Martinique lavas: A record of Lesser Antilles arc activity from 2Ma to Mount Pelée volcanism. Quaternary Geochronology. 6(3):341–355. doi:10.1016/j.quageo.2011.02.001.

Girina OA. 2013. Chronology of Bezymianny volcano activity, 1956–2010. Journal of Volcanology and Geothermal Research. 263:22–41.

Glicken H. 1996. Rockslide-debris avalanche of May 18, 1980, Mount St. Helens volcano, Washington. US Geological Survey, Cascades Volcano Observatory.

Gorbach N, Portnyagin M, Tembrel I. 2013. Volcanic structure and composition of Old Shiveluch volcano, Kamchatka. Journal of Volcanology and Geothermal Research. 263:193–208. doi:10.1016/j.jvolgeores.2012.12.012.

Gorshkov GS. 1959. Gigantic eruption of the volcano bezymianny. Bulletin Volcanologique. 20(1):77–109. doi:10.1007/BF02596572.

Gudmundsson A, Oskarsson N, Gronvold K, Saemundsson K, Sigurdsson O, Stefansson R, Gislason SR, Einarsson P, Brandsdottir B, Larsen G, et al. 1992. The 1991 eruption of Hekla, Iceland. Bulletin of Volcanology. 54(3):238–246. doi:10.1007/BF00278391.

Hall ML, Robin C, Beate B, Mothes P, Monzier M. 1999. Tungurahua Volcano, Ecuador: structure, eruptive history and hazards. Journal of Volcanology and Geothermal Research. 91(1):1–21. doi:10.1016/S0377-0273(99)00047-5.

Hausback BP, Swanson DA. 1990. Record of prehistoric debris avalanches on the North Flank of Mount St. Helens Volcano, Washington. Geoscience Canada. 17(3):142–145. https://journals.lib.unb.ca/index.php/GC/article/view/3666.

Hora JM, Singer BS, Wörner G, Beard BL, Jicha BR, Johnson CM. 2009. Shallow and deep crustal control on differentiation of calc-alkaline and tholeiitic magma. Earth and Planetary Science Letters. 285(1):75–86. doi:10.1016/j.epsl.2009.05.042.

Hornig-Kjarsgaard I. 1993. Geology, stratigraphy and volcanological evolution of the island of Stromboli, Aeolian arc, Italy. Acta Vulcanologica. 3:21–68. https://cir.nii.ac.jp/crid/1570572699956686080.

Höskuldsson Á, Óskarsson N, Pedersen R, Grönvold K, Vogfjörð K, Ólafsdóttir R. 2007. The millennium eruption of Hekla in February 2000. Bulletin of Volcanology. 70(2):169–182. doi:10.1007/s00445-007-0128-3.

Houghton B, Carey RJ. 2015. Pyroclastic fall deposits. In: Sigurdsson H, editor. The encyclopedia of volcanoes. Amsterdam: Elsevier; p. 599–616. https://doi.org/10.1016/B978-0-12-385938-9.00034-1.

Ingram RL. 1954. Terminology for the thickness of stratification and parting units in sedimentary rocks. Geological Society of America Bulletin. 65(9):937–938.

Johnson RW. 1987. Large-scale volcanic cone collapse: the 1888 slope failure of Ritter volcano, and other examples from Papua New Guinea. Bulletin of Volcanology. 49(5):669–679. doi:10.1007/BF01080358.

Karstens J, Berndt C, Urlaub M, Watt SFL, Micallef A, Ray M, Klaucke I, Muff S, Klaeschen D, Kühn M, et al. 2019. From gradual spreading to catastrophic collapse – reconstruction of the 1888 Ritter Island volcanic sector collapse from high-resolution 3D seismic data. Earth and Planetary Science Letters. 517:1–13. doi:10.1016/j.epsl.2019.04.009.

Katsui Y, Komuro H, Uda T. 1985. Development of faults and growth of Usu-Shinzan cryptodome in 1977–1982 at Usu Volcano, North Japan. 北海道大学理学部紀要. 21(3):339–362.

Katsui Y, Yamamoto M. 1981. The 1741–1742 Activity of Oshima-Ōshima Volcano, North Japan. J. Fac. Sci. Hokkaido Univ., Ser.4. 19(4):527–536. http://hdl.handle.net/2115/36702.

Keigler R, Thouret J-C, Hodgson KA, Neall VE, Lecointre JA, Procter JN, Cronin SJ. 2011. The Whangaehu formation: debris-avalanche and lahar deposits from ancestral Ruapehu volcano, New Zealand. Geomorphology. 133(1):57–79. doi:10.1016/j.geomorph.2011.06.019.

Land Information New Zealand. n.d. LINZ Data Service. https://data.linz.govt.nz/.

Lerner GA, Cronin SJ, Bebbington MS, Platz T. 2019c. The characteristics of a multi-episode volcanic regime: the post-AD 960 Maero Eruptive Period of Mt. Taranaki (New Zealand). Bulletin of Volcanology. 81(11):61. doi:10.1007/s00445-019-1327-4.

Lerner GA, Cronin SJ, Turner GM. 2019a. Evaluating emplacement temperature of a 1000-year sequence of mass flows using paleomagnetism of their deposits at Mt. Taranaki, New Zealand. Volcanica. 2(1):11–24.

Lerner GA, Cronin SJ, Turner GM, Piispa EJ. 2019b. Recognizing long-runout pyroclastic flow deposits using paleomagnetism of ash. GSA Bulletin. 131(11-12):1783–1793. doi:10.1130/b35029.1.

Luhr JF, Prestegaard KL. 1988. Caldera formation at Volcán Colima, Mexico, by a large large holocene volcanic debris

avalanche. Journal of Volcanology and Geothermal Research. 35(4):335–348. doi:10.1016/0377-0273(88)90027-3.

Lundgren P, Casu F, Manzo M, Pepe A, Berardino P, Sansosti E, Lanari R. 2004. Gravity and magma induced spreading of Mount Etna volcano revealed by satellite radar interferometry. Geophysical Research Letters. 31(4):1–4. https://doi.org/10.1029/2003GL018736.

Macedonio G, Dobran F, Neri A. 1994. Erosion processes in volcanic conduits and application to the AD 79 eruption of Vesuvius. Earth and Planetary Science Letters. 121(1):137–152. doi:10.1016/0012-821X(94)90037-X.

Manconi A, Longpré M-A, Walter TR, Troll VR, Hansteen TH. 2009. The effects of flank collapses on volcano plumbing systems. Geology. 37(12):1099–1102. doi:10.1130/g30104a.1.

Mastin LG, Guffanti M, Servranckx R, Webley P, Barsotti S, Dean K, Durant A, Ewert JW, Neri A, Rose WI, et al. 2009. A multidisciplinary effort to assign realistic source parameters to models of volcanic ash-cloud transport and dispersion during eruptions. Journal of Volcanology and Geothermal Research. 186(1):10–21. doi:10.1016/j.jvolgeores.2009.01.008.

McDonald GW, Cronin SJ, Kim JH, Smith NJ, Murray CA, Procter JN. 2017. Computable general equilibrium modelling of economic impacts from volcanic event scenarios at regional and national scale, Mt. Taranaki, New Zealand. Bulletin of Volcanology. 79(12):87. doi:10.1007/s00445-017-1171-3.

McEwen AS, Malin MC. 1989. Dynamics of Mount St. Helens' 1980 pyroclastic flows, rockslide-avalanche, lahars, and blast. Journal of Volcanology and Geothermal Research. 37(3):205–231. doi:10.1016/0377-0273(89)90080-2.

McGuire W. 2003. Volcano instability and lateral collapse. Revista. 1:33–45.

McGuire WJ. 1996. Volcano instability: a review of contemporary themes. Geological Society of London Special Publications. 110:1–23. doi:10.1144/gsl.Sp.1996.110.01.01.

Minakami T, Ishikawa T, Yagi K. 1951. The 1944 eruption of volcano Usu in Hokkaido, Japan. Bulletin Volcanologique. 11(1):45–157. doi:10.1007/BF02596029.

Moriya I. 1980. Bandaian eruption and landforms associated with it. In: Collection of articles in memory of retirement of Prof. K. Nishimura from Tohoku University. Sendai: Fac Sci Tohoku Univ; p. 214–219.

Neall V. 1979. Sheets P19, P20, and P21 New Plymouth, Egmont, and Manaia: New Zealand. Department of Scientific and Industrial Research.

Neall VE. 1972. Tephrochronology and tephrostratigraphy of western Taranaki (N108–109), New Zealand. New Zealand Journal of Geology and Geophysics. 15(4):507–557. doi:10.1080/00288306.1972.10423983.

Neall VE, Stewart RB, Smith IEM. 1986. History and petrology of the Taranaki volcanoes. In: Smith IEM, editor. Late Cenozoic volcanism. Royal Society of New Zealand Bulletin 23: 251–263.

Newhall CG, Self S. 1982. The Volcanic Explosivity Index (VEI): an estimate of explosive magnitude for historical volcanism. Journal of Geophysical Research. 87:1231–1238. doi:10.1029/JC087iC02p01231.

O'Callaghan L, Francis P. 1986. Volcanological and petrological evolution of San Pedro volcano, Provincia EI Loa, North Chile. Journal of the Geological Society. 143(2):275–286. doi:10.1144/gsjgs.143.2.0275.

Pallister JS, Clynne MA, Wright HM, Van Eaton AR, Vallance JW, Sherrod DR, Kokelaar BP. 2017. Field-trip guide to Mount St. Helens, Washington – an overview of the eruptive history and petrology, tephra deposits, 1980 pyroclastic density current deposits, and the crater [Report] (2017–5022D). (Scientific Investigations Report, Issue. U. S. G. Survey. https://pubs.usgs.gov/publication/sir20175022D.

Palmer BA, Alloway BV, Neall VE. 1991. Volcanic-debris-avalanche deposits in New Zealand—lithofacies organization in unconfined, wet-avalanche flows.

Paredes-Mariño J, Scheu B, Montanaro C, Arciniega-Ceballos A, Dingwell DB, Perugini D. 2019. Volcanic ash generation: effects of componentry, particle size and conduit geometry on size-reduction processes. Earth and Planetary Science Letters. 514:13–27. doi:10.1016/j.epsl.2019.02.028.

Petrone CM, Braschi E, Francalanci L. 2009. Understanding the collapse–eruption link at Stromboli, Italy: a micro-analytical study on the products of the recent Secche di Lazzaro phreatomagmatic activity. Journal of Volcanology and Geothermal Research. 188(4):315–332. doi:10.1016/j.jvolgeores.2009.09.016.

Pillans B. 1990. Pleistocene marine terraces in New Zealand: a review. New Zealand Journal of Geology and Geophysics. 33(2):219–231. doi:10.1080/00288306.1990.10425680.

Pinel V, Albino F. 2013. Consequences of volcano sector collapse on magmatic storage zones: insights from numerical modeling. Journal of Volcanology and Geothermal Research. 252:29–37. doi:10.1016/j.jvolgeores.2012.11.009.

Pinel V, Jaupart C. 2005. Some consequences of volcanic edifice destruction for eruption conditions. Journal of Volcanology and Geothermal Research. 145(1):68–80. doi:10.1016/j.jvolgeores.2005.01.012.

Platz T, Cronin SJ, Cashman KV, Stewart RB, Smith IEM. 2007. Transition from effusive to explosive phases in andesite eruptions — a case-study from the AD1655 eruption of Mt. Taranaki, New Zealand. Journal of Volcanology and Geothermal Research. 161(1):15–34. doi:10.1016/j.jvolgeores.2006.11.005.

Platz T, Cronin SJ, Procter JN, Neall VE, Foley SF. 2012. Non-explosive, dome-forming eruptions at Mt. Taranaki, New Zealand. Geomorphology. 136(1):15–30. doi:10.1016/j.geomorph.2011.06.016.

Ponomareva VV, Melekestsev IV, Dirksen OV. 2006. Sector collapses and large landslides on late Pleistocene–Holocene volcanoes in Kamchatka, Russia. Journal of Volcanology and Geothermal Research. 158(1):117–138. doi:10.1016/j.jvolgeores.2006.04.016.

Procter J, Cronin S, Zernack A. 2009. Landscape and sedimentary response to catastrophic debris avalanches, western Taranaki, New Zealand. Sedimentary Geology. 220(3):271–287. doi:10.1016/j.sedgeo.2009.04.027.

Pyle DM. 1989. The thickness, volume and grainsize of tephra fall deposits. Bulletin of Volcanology. 51(1):1–15. doi:10.1007/BF01086757.

Pyle DM. 1995. Assessment of the minimum volume of tephra fall deposits. Journal of Volcanology and Geothermal Research. 69(3):379–382. doi:10.1016/0377-0273(95)00038-0.

Pyle DM. 2000. The sizes of volcanic eruptions. In: Sigurdsson H, Houghton B, McNutt SR, Rymer H, Stix J, editors. Encyclopedia of volcanoes. London, UK: Academic Press; p. 263–269.

Robin C, Komorowski J-C, Boudal C, Mossand P. 1990. Mixed-magma pyroclastic surge deposits associated with debris avalanche deposits at Colima volcanoes, Mexico. Bulletin of Volcanology. 52(5):391–403. doi:10.1007/BF00302051.

Rose WI. 1993. Comment on 'another look at the calculation of fallout tephra volumes' by Judy Fierstein and Manuel Nathenson. Bulletin of Volcanology. 55(5):372–374.

Rosi M, Principe C, Vecci R. 1993. The 1631 Vesuvius eruption. A reconstruction based on historical and stratigraphical data. Journal of Volcanology and Geothermal Research. 58(1):151–182. doi:10.1016/0377-0273(93)90106-2.

Roverato M, Di Traglia F, Procter J, Paguican E, Dufresne A. 2021. Factors contributing to volcano lateral collapse. In: Roverato M, Dufresne A, Procter J, editors. Volcanic debris avalanches: from collapse to hazard. Cham: Springer International Publishing. p. 91–119. doi:10.1007/978-3-030-57411-6_5.

Roverato M, Dufresne A. 2021. Volcanic debris avalanches: introduction and book structure. In: Roverato M, Dufresne A, Procter J, editors. Volcanic debris avalanches. Cham: Springer; p. 1–10.

Sarna-Wojcicki AM. 1981. Areal distribution, thickness, mass, volume, and grain size of air-fall ash from the six major eruptions of 1980. In: Lipman PW, Mullineaux DR, editors. The 1980 eruptions of Mount St. Helens. Washington: U.S. Geological Survey; p. 577–601. https://cir.nii.ac.jp/crid/1571417124294377344.

Satake K. 2007. Volcanic origin of the 1741 Oshima-Oshima tsunami in the Japan Sea. Earth, Planets and Space. 59(5):381–390. doi:10.1186/BF03352698.

Satake K, Kato Y. 2001. The 1741 Oshima-Oshima Eruption: extent and volume of submarine debris avalanche. Geophysical Research Letters. 28:427–430. doi:10.1029/2000gl012175.

Scandone R, Malone SD. 1985. Magma supply, magma discharge and readjustment of the feeding system of mount St. Helens during 1980. Journal of Volcanology and Geothermal Research. 23(3):239–262. doi:10.1016/0377-0273(85)90036-8.

Schaaf P, Carrasco-Núñez G. 2010. Geochemical and isotopic profile of Pico de Orizaba (Citlaltépetl) volcano, Mexico: Insights for magma generation processes. Journal of Volcanology and Geothermal Research. 197(1):108–122. doi:10.1016/j.jvolgeores.2010.02.016.

Scott KM, Vallance J, Pringle PT. 1995. Sedimentology, behavior, and hazards of debris flows at Mount Rainier, Washington. Professional Paper. doi:10.3133/pp1547.

Scott KM, Vallance JW, Kerle N, Luis Macías J, Strauch W, Devoli G. 2005. Catastrophic precipitation-triggered lahar at Casita volcano, Nicaragua: occurrence, bulking and transformation. Earth Surface Processes and Landforms. 30:59–79. doi:10.1002/esp.1127.

Shea T, van Wyk de Vries B, Pilato M. 2008. Emplacement mechanisms of contrasting debris avalanches at Volcán Mombacho (Nicaragua), provided by structural and facies analysis. Bulletin of Volcanology. 70(8):899–921. doi:10.1007/s00445-007-0177-7.

Sherrod DR, Vallance JW, Espinosa AT, McGeehin JP. 2007. Volcán Barú—Eruptive history and volcano-hazards assessment. US Geological Survey Open-File Report, 2007, 1401.

Siebert L. 1996. Hazards of large volcanic debris avalanches and associated eruptive phenomena. In: Scarpa R, Tilling RI, editors. Monitoring and mitigation of volcanic hazards. Heidrlberg, Berlin: Springer; p. 541–572. https://cir.nii.ac.jp/crid/1572824498950008576.

Siebert L, Glicken H, Ui T. 1987. Volcanic hazards from Bezymianny- and Bandai-type eruptions. Bulletin of Volcanology. 49(1):435–459. doi:10.1007/BF01046635.

Siebert L, Kimberly P, Pullinger CR, Rose WI, Bommer JJ, López DL, Carr MJ, Major JJ. 2004. The voluminous Acajutla debris avalanche from Santa Ana volcano, western El Salvador, and comparison with other Central American edifice-failure events. In: Rose WI, Bommer JJ, López DL, Carr MJ, Major JJ, editors. Natural hazards in El Salvador. Vol. 375. Boulder, Colorado: Geological Society of America; p. 5–23. doi:10.1130/0-8137-2375-2.5.

Sparks RSJ. 1976. Grain size variations in ignimbrites and implications for the transport of pyroclastic flows. Sedimentology. 23(2):147–188.

Stoopes GR, Sheridan MF. 1992. Giant debris avalanches from the Colima Volcanic Complex, Mexico: implications for long-runout landslides (>100 km) and hazard assessment. Geology. 20(4):299–302. doi:10.1130/0091-7613(1992)020<0299:Gdaftc>2.3.Co;2.

Taddeucci J, Wohletz KH. 2001. Temporal evolution of the Minoan eruption (Santorini, Greece), as recorded by its Plinian fall deposit and interlayered ash flow beds. Journal of Volcanology and Geothermal Research. 109(4):299–317. doi:10.1016/S0377-0273(01)00197-4.

Thorarinsson S, Sigvaldason GE. 1972. The Hekla Eruption of 1970. Bulletin Volcanologique. 36(2):269–288. doi:10.1007/BF02596870.

Tibaldi A. 2004. Major changes in volcano behaviour after a sector collapse: insights from Stromboli, Italy. Terra Nova. 16:2–8. doi:10.1046/j.1365-3121.2003.00517.x.

Tormey D. 2010. Managing the effects of accelerated glacial melting on volcanic collapse and debris flows: Planchon–Peteroa Volcano, Southern Andes. Global and Planetary Change. 74(2):82–90. doi:10.1016/j.gloplacha.2010.08.003.

Torres-Orozco R, Cronin SJ, Damaschke M, Pardo N. 2017b. Diverse dynamics of Holocene mafic-intermediate Plinian eruptions at Mt. Taranaki (Egmont), New Zealand. Bulletin of Volcanology. 79(11):76. doi:10.1007/s00445-017-1162-4.

Torres-Orozco R, Cronin SJ, Pardo N, Palmer AS. 2017a. New insights into Holocene eruption episodes from proximal deposit sequences at Mt. Taranaki (Egmont), New Zealand. Bulletin of Volcanology. 79(1):3. doi:10.1007/s00445-016-1085-5.

Torres-Orozco R, Cronin SJ, Pardo N, Palmer AS. 2018. Volcanic hazard scenarios for multiphase andesitic Plinian eruptions from lithostratigraphy: Insights into pyroclastic density current diversity at Mount Taranaki, New Zealand. GSA Bulletin. 130(9-10):1645–1663. doi:10.1130/b31850.1.

Tost M, Cronin SJ. 2016. Climate influence on volcano edifice stability and fluvial landscape evolution surrounding Mount Ruapehu, New Zealand. Geomorphology. 262:77–90. doi:10.1016/j.geomorph.2016.03.017.

Tost M, Cronin SJ, Procter JN. 2014. Transport and emplacement mechanisms of channelised long-runout debris avalanches, Ruapehu volcano, New Zealand. Bulletin of Volcanology. 76(12):881. doi:10.1007/s00445-014-0881-z.

Turner MB, Cronin SJ, Smith IE, Stewart RB, Neall VE. 2008. Eruption episodes and magma recharge events in andesitic systems: Mt Taranaki, New Zealand. Journal of Volcanology and Geothermal Research. 177(4):1063–1076. doi:10.1016/j.jvolgeores.2008.08.001.

Udden JA. 1914. Mechanical composition of clastic sediments. Bulletin of the Geological Society of America. 25(1):655–744.

Vallance JW, Schilling SP, Matías O, Rose WI, Jr, Howell MM. 2001. Volcano hazards at Fuego and Acatenango, Guatemala [Report] (2001-431). (Open-File Report,

Issue. U. S. G. Survey. https://pubs.usgs.gov/publication/ofr01431.
Vallance JW, Scott KM. 1997. The Osceola Mudflow from Mount Rainier: sedimentology and hazard implications of a huge clay-rich debris flow. GSA Bulletin. 109(2):143–163. doi:10.1130/0016-7606(1997)109<0143:Tomfmr>2.3.Co;2.
Vallance JW, Siebert L, Rose WI, Girón JR, Banks NG. 1995. Edifice collapse and related hazards in Guatemala. Journal of Volcanology and Geothermal Research. 66(1):337–355. doi:10.1016/0377-0273(94)00076-S.
Vandergoes MJ, Hogg AG, Lowe DJ, Newnham RM, Denton GH, Southon J, Barrell DJA, Wilson CJN, McGlone MS, Allan ASR, et al. 2013. A revised age for the Kawakawa/Oruanui tephra, a key marker for the Last Glacial Maximum in New Zealand. Quaternary Science Reviews. 74:195–201. doi:10.1016/j.quascirev.2012.11.006.
van Wyk de Vries B, Self S, Francis PW, Keszthelyi L. 2001. A gravitational spreading origin for the Socompa debris avalanche. Journal of Volcanology and Geothermal Research. 105(3):225–247. doi:10.1016/S0377-0273(00)00252-3.
Varekamp JC. 1993. Some remarks on volcanic vent evolution during Plinian eruptions. Journal of Volcanology and Geothermal Research. 54(3):309–318. doi:10.1016/0377-0273(93)90069-4.
Vezzoli L, Renzulli A, Menna M. 2014. Growth after collapse: the volcanic and magmatic history of the Neostromboli lava cone (island of Stromboli, Italy). Bulletin of Volcanology. 76(6):821. doi:10.1007/s00445-014-0821-y.
Voight B. 2000. Structural stability of andesite volcanoes and lava domes. Philosophical Transactions of the Royal Society of London. Series A: Mathematical, Physical and Engineering Sciences. 358(1770):1663–1703. doi:10.1098/rsta.2000.0609.
Voight B, Elsworth D. 1997. Failure of volcano slopes. Geotechnique. 47(1):1–31. doi:10.1680/geot.1997.47.1.1.
Voight B, Glicken H, Janda RJ, Douglass PM. 1980. Catastrophic rockslide avalanche of May 18. The, 1250, 347.
Voight B, Glicken H, Janda RJ, Douglass PM. 1981. Catastrophic rockslide avalanche of May 18. In: Lipman PW, Mullineaux DR, editors. The 1980 eruptions of Mount St. Helens, Washington. US Geological Survey Professional Paper 1250. p. 347–377.
Voight B, Janda RJ, Glicken H, Douglass PM. 1983. Nature and mechanics of the Mount St Helens rockslide-avalanche of 18 May 1980. Geotechnique. 33(3):243–273. doi:10.1680/geot.1983.33.3.243.
Voight B, Komorowski JC, Norton GE, Belousov A, Belousova M, Boudon G, Francis PW, Franz W, Heinrich P, Sparks RSJ, Young SR. 2002. The 26 December (Boxing Day) 1997 sector colapse and debris avalanche at Soufriere Hills Volcano, Montserrat. In: Druitt TH, Kokelaar BP, editors. The eruption of Soufriere Hills Volcano, Montserrat, from 1995 to 1999. Memoirs-Geological Society of London, 21, 363–408.
Voloschina M, Lube G, Procter J, Moebis A, Timm C. 2020. Lithosedimentological and tephrostratigraphical characterisation of small-volume, low-intensity eruptions: The 1800 years Tufa Trig Formation, Mt. Ruapehu (New Zealand). Journal of Volcanology and Geothermal Research. 402:106987. doi:10.1016/j.jvolgeores.2020.106987.
Watt SFL. 2019. The evolution of volcanic systems following sector collapse. Journal of Volcanology and Geothermal Research. 384:280–303. doi:10.1016/j.jvolgeores.2019.05.012.
Weir AM, Mead S, Bebbington MS, Wilson TM, Beaven S, Gordon T, Campbell-Smart C. 2022. A modular framework for the development of multi-hazard, multi-phase volcanic eruption scenario suites. Journal of Volcanology and Geothermal Research. 427:107557. doi:10.1016/j.jvolgeores.2022.107557.
Wentworth CK. 1922. A scale of grade and class terms for clastic sediments. Journal of Geology. 30:377–392. doi:10.1086/622910.
White JDL, Houghton BF. 2006. Primary volcaniclastic rocks. Geology. 34(8):677–680. doi:10.1130/g22346.1.
Wilson L. 1976. Explosive volcanic eruptions—III. Plinian eruption columns. Geophysical Journal International. 45(3):543–556.
Yamamoto T, Nakamura Y, Glicken H. 1999. Pyroclastic density current from the 1888 phreatic eruption of Bandai volcano, NE Japan. Journal of Volcanology and Geothermal Research. 90(3):191–207. doi:10.1016/S0377-0273(99)00025-6.
Yoshida H. 2013. Decrease of size of hummocks with downstream distance in the rockslide-debris avalanche deposit at Iriga volcano, Philippines: similarities with Japanese avalanches. Landslides. 10(5):665–672. doi:10.1007/s10346-013-0414-4.
Zemeny A, Procter J, Nemeth K, Zellmer GF, Zernack AV, Cronin SJ. 2021. Elucidating stratovolcano construction from volcaniclastic mass-flow deposits: The medial ring-plain of Taranaki Volcano, New Zealand. Sedimentology. 68:2422–2449.
Zemeny A, Zellmer GF, Ubide T, Smith IEM, Procter J, Tapu A-T, Zernack AV. 2023. Investigation of the Mid-Age (65–34 ka) Period of Taranaki Volcano, New Zealand: indications for the Effect of Volcano Growth. Journal of Petrology. 64(5):1–21. doi:10.1093/petrology/egad027.
Zernack AV. 2021. Volcanic debris-avalanche deposits in the context of volcaniclastic ring plain successions—a case study from Mt. Taranaki. In: Roverato M, Dufresne A, Procter J, editors. Volcanic debris avalanches: from collapse to hazard. Cham: Springer International Publishing. p. 211–254. doi:10.1007/978-3-030-57411-6_9.
Zernack AV, Cronin SJ, Bebbington MS, Price RC, Smith IEM, Stewart RB, Procter JN. 2012. Forecasting catastrophic stratovolcano collapse: a model based on Mount Taranaki, New Zealand. Geology. 40(11):983–986. doi:10.1130/g33277.1.
Zernack AV, Cronin SJ, Neall VE, Procter JN. 2011. A medial to distal volcaniclastic record of an andesite stratovolcano: detailed stratigraphy of the ring-plain succession of south-west Taranaki, New Zealand. International Journal of Earth Sciences. 100(8):1937–1966. doi:10.1007/s00531-010-0610-6.
Zernack AV, Procter JN. 2021. Cyclic growth and destruction of volcanoes. In: Roverato M, Dufresne A, Procter J, editors. Volcanic debris avalanches: from collapse to hazard. Cham: Springer International Publishing. p. 311–355. doi:10.1007/978-3-030-57411-6_12.
Zernack AV, Procter JN, Cronin SJ. 2009. Sedimentary signatures of cyclic growth and destruction of stratovolcanoes: a case study from Mt. Taranaki, New Zealand. Sedimentary Geology. 220(3):288–305. doi:10.1016/j.sedgeo.2009.04.024.